LITHOS 534–535 (2026) 108546

Contents lists available at ScienceDirect

LITHOS

journal homepage: www.elsevier.com/locate/lithos

Melt-rock interaction driving extreme titanium and vanadium enrichments during the multi-stage post-magmatic evolution of chromite from the Mirdita Ophiolite, Kosovo

Micol Bussolesi [a,b,*], Giovanni Grieco [b], Alessandro Cavallo [a], Qazim Hyseni [c], Federico Farina [b]

[a] Department of Earth and Environmental Sciences - DISAT, University of Milan-Bicocca, P.zza della Scienza 1, 20126 Milan, Italy
[b] Department of Earth Sciences, University of Milan, via Botticelli 23, 20133 Milan, Italy
[c] Department of Applied Geology and Geophysics, Goce Delcev University, Shtip, Macedonia

ARTICLE INFO

Keywords:
Ti- V-rich chromite
Melt-rock reaction
Rodingite
Mediterranean ophiolite
PCA

ABSTRACT

Chromitites associated with rodingite from the Deva mining district (Mirdita Ophiolite, Kosovo) display thick reaction rims at the contact between chromite and silicate matrix. The most peculiar feature of these rims is an anomalous enrichment in titanium (Ti) and vanadium (V) in the chromite, alongside the presence of abundant rutile, ilmenite and titanite. The integration of textural and mineralogical observations, minero-chemical data and statistical analysis, through Principal Component Analysis (PCA), reveals a complex evolution of the chromitite body and its host rocks. Primary chromitites formed in a supra-subduction zone forearc environment, from melts with boninitic affinity. The subsequent intrusion of a mafic body and its interaction with the chromitites led to significant enrichments in Ti, V and minor Ga, Ni and Mn in chromite. At lower temperature, Ti was partially exsolved to form Ti-phases. During a later serpentinization event affecting the ophiolite mantle rocks, the circulation of reducing hydrothermal fluids caused the rodingitization of the mafic intrusion, replacing primary silicates with hydrogrossular, clinopyroxene and chlorite. While serpentinization and rodingitization only marginally affected the chromitite body, they caused local Al re-enrichment in the previously depleted spinel rims due to the liberation of Aluminum during plagioclase break-up. The study highlights the complexity of superimposed magmatic and low-temperature processes capable of modifying chromite chemistry and emphasizes the importance of integrated approaches in unraveling their individual contributions.

1. Introduction

Spinels form a broad mineral group defined by multiple end-members and a wide variety of solid solutions, resulting in highly variable chemical compositions. As spinel chemistry records the physico-chemical conditions during crystallization, including temperature, pressure and oxygen fugacity, as well as subsequent subsolidus re-equilibration, these minerals are widely used as petrogenetic indicators (Dilek et al., 2008; Irvine, 1965; Sack and Ghiorso, 1991). Spinel is the most common accessory phase in mantle peridotites, remaining stable across a wide range of pressures and being replaced by plagioclase and garnet only at very low and very high-pressure respectively, outside of the typical stability field of the upper mantle. Upper mantle spinel is typically chromiferous, with Cr^{3+} occupying octahedral sites and Mg^{2+} tetrahedral sites. Extensive cation substitutions (Fe^{3+} and Al^{3+} for Cr^{3+} and Fe^{2+} for Mg^{2+}) make spinel a valuable petrogenetic indicator of upper mantle evolution processes, including partial melting, melt upward transfer, metasomatism, melt evolution and crystallization. As chromite is largely affected by changes in sub-solidus conditions it also records post magmatic processes such as cooling, metamorphism or hydrothermal alteration (Bussolesi et al., 2022a; Ghosh and Morishita, 2011; Grieco and Merlini, 2012; Merlini et al., 2009; Sideridis et al., 2022).

Despite numerous studies on major-element systematics in chromite, reconstructing its full compositional evolution, from crystallization to late-stage modifications, remains challenging. Among the processes that can lead to substantial changes in spinel mineral chemistry there are interaction with intercumulus liquid (Barnes and Kunilov, 2000), post-crystallization alteration such as oxidation-exsolution of ilmenite (Abzalov, 1998), subsolidus exchange with primary silicates (Ballhaus

* Corresponding author at: Department of Earth Sciences, University of Milan, via Botticelli 23, 20133 Milan, Italy.
E-mail address: micol.bussolesi@unimi.it (M. Bussolesi).

https://doi.org/10.1016/j.lithos.2026.108546
Received 17 November 2025; Received in revised form 27 March 2026; Accepted 2 April 2026
Available online 7 April 2026

et al., 1991; Bussolesi et al., 2019; Fabriès, 1979; Ozawa, 1984) and low temperature alterations (Kimball, 1990; Merlini et al., 2009). In this framework, investigating trace element contents in spinel can lead to a thorough understanding of the processes affecting chromite compositional changes. Several detailed studies have explored the application of trace element in chromite to constrain magmatic processes and mantle melting (Barnes and Roeder, 2001; González-Jiménez et al., 2014; Page and Barnes, 2009). Trace element datasets are also available for spinels in ophiolitic chromitites (González-Jiménez et al., 2015; Proenza et al., 1999; Zhou et al., 2014), although comparatively few studies have addressed how trace elements in chromite are affected during metamorphism or other post-magmatic modifications (Barnes and Roeder, 2001; Colás et al., 2014; González-Jiménez et al., 2009).

Chromite can incorporate a suite of minor and trace elements including scandium (Sc), titanium (Ti), vanadium (V), manganese (Mn), cobalt (Co), nickel (Ni), zinc (Zn), and gallium (Ga). The concentrations of these elements vary significantly depending on several factors, including the degree of partial melting, melt-peridotite reactions and post-magmatic processes (Barnes et al., 2023; Page and Barnes, 2009). Chromite in ophiolitic chromitites is generally Ti-, Ga- and Ni-poor, with relatively flat trace element patterns compared to MORB chromite, consistent with high-degree melting and a forearc boninitic affinity. In contrast, Ti enrichment in spinels is more commonly associated with MORB-like lavas (Page and Barnes, 2009). Enrichments in Zn, Co and Mn, and depletion in Ga, Ni, Sc and V in ophiolitic chromites are typically associated to metamorphic overprinting and fluid-related modifications (Colás et al., 2014).

This study investigates the petrogenetic information recorded in chromite major, minor and trace element compositions, focusing on melt-rock reaction and metamorphic processes affecting chromitites. Major cation substitution involving elements typically present in trace amounts are explored using statistical tools, specifically Principal Component Analysis, to reduce the number of variables and extract more information from the dataset. Deva chromitites provide an ideal testing ground, as they exhibit both magmatic and post-magmatic features in a complex geological setting characterized by a wide range of spinel compositions.

2. Geological setting

The Western Balkan ophiolites form part of the Late Jurassic Tethyan ophiolitic belt. They extend across the Balkans, through Central Serbia, Kosovo, Albania, North Makedonia to Northern Greece (Çina, 2018). The study area is located in southwest Kosovo, within the Deva municipality, near the border with Albania. These ophiolites host significant chromite deposits and several abandoned mines. One of these, Queen Mine 1, was selected as the sampling site, with samples collected from ore bodies and waste heaps outside the main tunnel adit. The Deva chromitite deposits are geologically hosted in the Gjakova-Tropoje massif (also referred to as the Tropoje massif) which forms part of the Mirdita Ophiolite (Fig. 1). This ophiolite represents remnants of the oceanic lithosphere of the Pindos-Mirdita basin (Bortolotti et al., 1996; Dilek et al., 2005), and forms a NNW-SSE trending belt of ultramafic massifs. Based on petrological and geochemical characteristics, the Mirdita ophiolites are broadly divided into two main belts: the Western-type Mirdita ophiolites (WMO) and the Eastern-type Mirdita ophiolites (EMO) (Saccani et al., 2011; Saccani and Tassinari, 2015).

The EMO, comprising the Kukes, Tropoje, Lure and Bulquiza massifs, consist of depleted harzburgites and dunites hosting abundant chromitite bodies. At the base of the Tropoje stratigraphic sequence lie variably depleted harzburgites, often containing dunite and chromitite pods and lenses that increase in abundance upwards. These mantle lithologies are overlain by ultramafic cumulates, including dunites with chromitite layers, olivine-websterites, and websterites, exhibiting a typical SSZ-type crystallization order (olivine ± chromite, pyroxenes + plagioclase + magnetite, ilmenite). Locally, plagioclase-lherzolites and

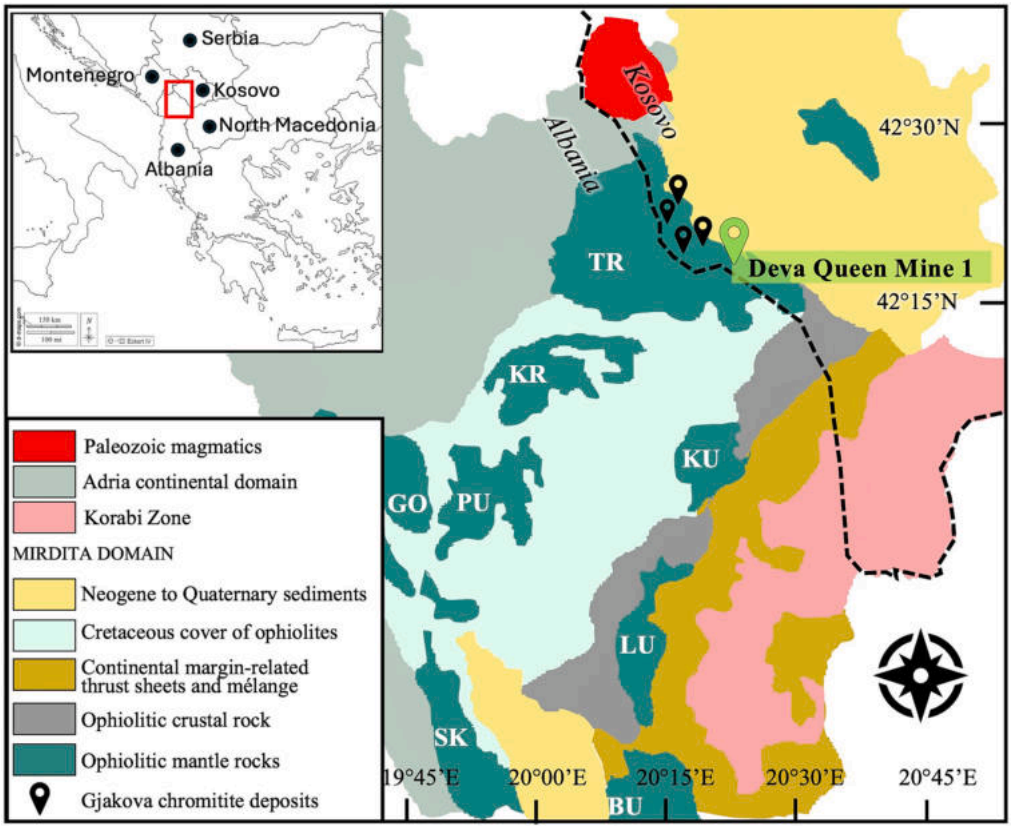

Fig. 1. Simplified geological map of the study area, highlighting the location of Deva Queen Mine 1 chromitites within the Mirdita Domain in Kosovo.

troctolites layers are also present. Above these units, cumulitic mafic rocks are largely dominated by olivine-gabbronorites and gabbronorites, followed by abundant quartz-diorites and plagiogranites. The EMO further includes a thick sheeted dyke complex and a volcanic sequence comprising basalts, basaltic andesites, andesites, dacites, and rhyolites, displaying mainly Island Arc Tholeiite (low-Ti) and boninitic (very low-Ti) affinities, although occurrences of high-Ti magmatism have also been reported. These volcanic rocks occur as both massive and pillow lavas and are frequently crosscut by boninitic dykes (Saccani and Tassinari, 2015).

3. Materials and methods

3.1. Samples and locations

Chromitite occurrences and deposits have been identified in several regions of Kosovo, but the Gjakova mining district is the best known. By 2017, when mining operations ceased, approximately 1 M tons of chromite ore, with an average grade of 44 wt% Cr_2O_3, had been extracted. Nowadays, due to the scarcity of chromitite outcrops and the inaccessibility of mining tunnels, representative chromitite samples can only be collected from minor residual stocks located in the Deva area. The collected specimens, including both massive and disseminated chromitites, were collected from a small stock at the abandoned Queen 1 mine (N 42°19′54″, E 20°20′49″) (Fig. 1). In addition, silicate host rocks were sampled from altered peridotite outcrops located outside the tunnel adit. A total of 24 samples were collected, of which 9 were selected for textural observations and subsequent analytical investigations as representative of the variability in texture and mineralogy (Table 1).

3.2. Mineral chemistry

Mineral chemistry of silicates and oxides was determined through electron micro probe analyzer (EMPA) at the Unitech COSPECT facility of the University of Milan (Italy). The probe is a JXA 8200 superprobe, equipped with a wavelength dispersive system. Operating conditions included an accelerating voltage of 15 kV, a sample current on brass of 15 nA, and counting times of 20 s on the peaks and 10 s on the background. Standards used include wollastonite for Si, forsterite for Mg, ilmenite for Ti, fayalite for Fe, anorthite for Al and Ca, chromite for Cr, nickeline for Ni, rhodonite for Mn and Zn, and metallic V for that element. The approximate detection limit is 0.01 wt% for each element. Fe^{3+} was recalculated from microprobe analyses assuming perfect stoichiometry, based on 8-oxygen formula. Analyzed lines are all kα. Overlap corrections include V—Ti and Cr—V.

Complete mineral chemistry analyses are reported in Supplementary Material 1 (SM1), Table 1 (spinel), Table 2 (olivine), Table 3 (serpentine), Table 4 (clinopyroxene), Table 5 (garnet), Table 6 (chlorite), Table 7 (titanite, ilmenite, rutile). Principal Component Analysis computation is reported in SM1 Table 8.

Table 1
Chromitite and altered peridotite samples from Queen 1 abandoned mine, Deva area.

Sample	Mineralogy	Lithology
D-5	Chromite, serpentine	Massive chromitite
D-14	Chromite, chlorite, Cr-garnet	Massive chromitite
D-17	Chromite, hydrogrossular, chlorite, clinopyroxene, titanite, rutile, ilmenite, vesuvianite	Massive chromitite – Rodingite
D-18	Chromite, tremolite, chlorite	Massive chromitite – Altered peridotite
D-19	Chromite, orthopyroxene, clinopyroxene, chlorite, serpentine	Massive chromitite – Altered peridotite
D-20	Chromite, olivine, serpentine, brucite, dolomite	Disseminated chromitite
D-23	Serpentine, olivine, chromite, chlorite	Altered dunite
D-24	Clinopyroxene, hydrogrossular, chlorite, titanite, calcite, chromite, rutile	Chromitite nodule - rodingite

3.3. LA-ICP-MS

The concentration of minor and trace elements was determined by laser ablation inductively coupled plasma mass spectrometry (LA-ICP-MS) at the Geochemistry, Geochronology and Isotope Geology Laboratory of the Earth Sciences Department, University of Milan. The instrument couples 193 nm ArF excimer laser ablation microprobe (Analyte Excite from Teledyne Cetac Technologies) equipped with a double chamber ablation cell (HelEx II) with a single-collector quadrupole ICP-MS (iCAP RQ from Thermo Fisher Scientific). Before the analytical session, the instrument was tuned in linear scan mode on the NIST-SRM 612 silicate glass and oxide generation was mitigated by keeping the 140CeO+/140Ce + (with O referring to 16O) <0.3.

Silicate glass GSD2 was used for calibration. To account for instrumental drift, it was measured twice every 10 chromite analyses. The spot analyses were performed using a 10 Hz repetition rate and a laser output energy of 8.6 J/cm2 with an ablation spot size of 40 μm. Each analysis consisted of 40 s background measurement followed by 40 s of laser ablation. For concentration calculations, average background-subtracted count rates for each analyte were internally normalized to ^{57}Fe, previously determined by EMPA. Glasses ARM3–1 and BCR2-g were used as reference materials to determine accuracy together with chromite LBS13–04 from (Wang et al., 2023). These were analyzed once every 10 unknowns. The trace elements considered for the work are Sc, Ti, V, Mn, Co, Ni, Zn and Ga. The relative errors for these elements are generally within 10%, except for Sc (21% with ARM3 and − 33% for LBS13–04), and Zn (19% with BCR2). The raw data were processed and transformed into elemental contents using the GLITTER software package (Van Achterbergh et al., 1999).

Trace element concentrations are reported in Supplementary Material 2, Table 1 (SM2 Table 1). Quality control and accuracy are reported in SM2 Table 2, and Principal Component Analysis computation for trace element analyses is reported in SM2 Table 3.

3.4. Statistical procedure

Principal Component Analysis (PCA) is a multivariate statistical technique used to reduce the dimensionality of large datasets containing several inter-correlated variables. It transforms the original variables into a new set of orthogonal variables, called Principal Components, which are ordered such that that the first components account for most of the variance in the dataset (*Principal Component Analysis*, 2002). Each Principal Component is a linear combination of the original variables, with coefficients (loadings) derived from the eigenvectors of the covariance (or correlation) matrix. The following pre-processing and analytical steps were applied:

i. **Treatment of missing values:** Values below the detection limit were replaced by $\frac{1}{2}$ LOD (Limit of Detection). This step was applied only to trace element data, and affected a limited number of analyses.
ii. **Log-transformation:** Trace elements data were log-transformed (ln) to reduce skewness and approximate a normal distribution.
iii. **Standardization:** All data were standardized using the z-score method (subtracting the mean and dividing by the standard deviation), ensuring that each variable contributes equally to the PCA.
iv. **Covariance Matrix:** A covariance matrix was computed in order to evaluate correlations among variables.
v. **Eigenvectors and eigenvalues:** Eigenvectors and eigenvalues of the covariance matrix were calculated to define the Principal

Components. These computations were performed using a Python script (see SM3).

vi. **Data projection:** The dataset was recast along the principal component axes (see supplementary materials).

4. Results

4.1. Texture and mineralogy

Chromitite samples were collected from small residual stocks outside of the mine adit (Fig. 2a). The chromitites predominantly display massive textures, which, in some cases, gradually transition into densely disseminated ones. The contact between chromitites and their host rock is always sharp (Fig. 2b, c, d).

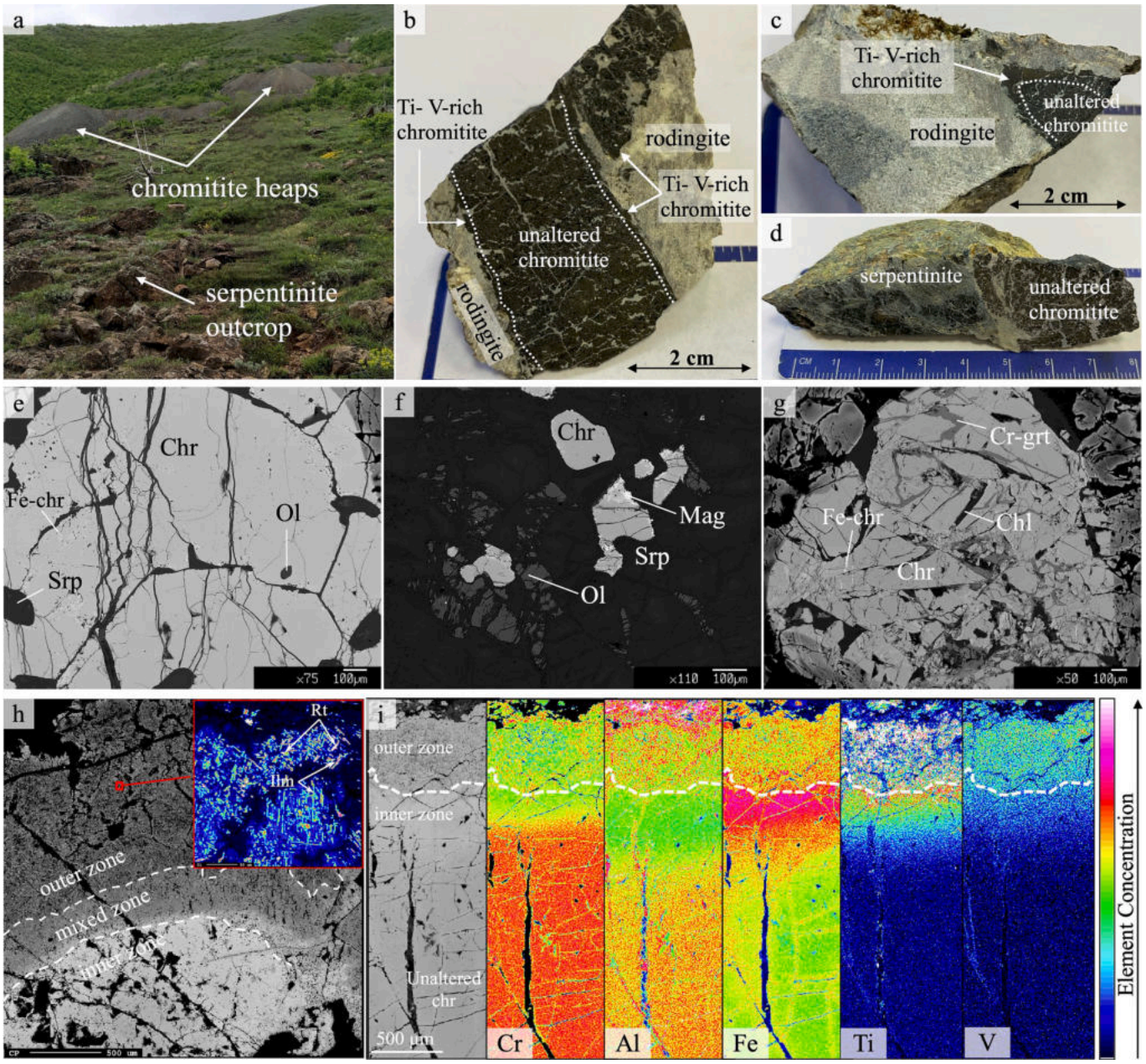

Fig. 2. Field, hand specimens and textural details (backscattered electron images, BSE) of studied chromitites and host serpentinite. (a) Field photograph showing chromitite heaps and serpentinized peridotite at Queen Mine 1; (b) Hand specimen displaying a massive chromitite with unaltered core surrounded by a Ti- V-rich rim, in contact with rodingite (sample D17); (c) Hand specimen showing a chromitite nodule with Ti- V-rich rim, in contact with rodingite (sample D24); (d) Hand specimen of unaltered massive chromitite enclosed in serpentinite, showing no evidence of Ti- V enrichment; (e) Massive chromitite showing chromite crystals with limited ferrian chromite, associated to crystal fracture, serpentine and olivine relict (sample D20); (f) altered peridotite showing dispersed chromite with magnetite rim, olivine and serpentine (sample D23); (g) Highly fractured massive chromitite (sample D14) with Cr-garnet growing along fractures in association with chlorite; (h) Outer, Mixed and Inner Zones of a chromitite nodule (sample D24). The red box highlights a 50μm x 50μm area rich in ilmenite and rutile exsolution lamellae; (i) BSE and elemental maps of a transect from chromite rim (Outer Zone) to core (Unaltered chromite) (sample D17). Mineral abbreviations are chr: chromite, Fe-chr: ferrian chromite, ol: olivine, srp: serpentine, mag: magnetite, ilm: ilmenite, rt.: rutile. (For interpretation of the references to colour in this figure legend, the reader is referred to the web version of this article.)

Most chromitite samples consist of subhedral, heavily fractured chromite crystals, showing widespread, even though volumetrically limited, alteration into ferrian chromite. The silicate matrix is serpentinized, with rare olivine relicts preserved (Fig. 2e). These chromitites are hosted within serpentinized dunite containing relict olivine and accessory chromite grains surrounded by magnetite coronae (Fig. 2f). Some chromitite samples display a more complex mineral assemblage, including uvarovitic garnet, which occurs along chromite fractures and at the interface between chromite and Cr-chlorite (Fig. 2g). Two samples show significant mineralogical complexity. They consist of centimetric chromitite nodules and layers in contact with a rodingite. The chromitite at the contact with rodingite exhibits thick reaction bands, here referred to, from the lithological contact inward, as Outer Zone, Mixed Zone and Inner Zone (Fig. 2h). The Outer Zone forms a thick reaction rim characterized by a "spongy" texture, pervasive fractures and the presence of ilmenite and rutile exsolution lamellae (Fig. 2h). The Mixed Zone is relatively thin and locally absent (Fig. 2i) and displays less pervasive alteration features compared to the Outer Zone (Fig. 2h). The Inner Zone lacks the distinctive textural features of the outer zone; however, chromite compositions still record evidence of reaction processes (Fig. 2h, i).

The rodingite is composed of clinopyroxene, hydrogrossular and chlorite, with accessory titanite, ilmenite and rutile (Fig. 3). Clinopyroxene is altered and partially replaced by chlorite (Fig. 3a, b). Mineral chemistry and BSE images reveal multiple clinopyroxene generations within rodingites, with a Fe-rich variety (cpx2) replacing an earlier, Fe-poor one (cpx1) (Fig. 3c, e, f). Hydrogrossular forms subhedral to anhedral grains in contact with clinopyroxene through reaction rims (Fig. 3d, f). Two compositionally distinct grossular garnets are present, with a Fe-rich variety (grt2) replacing a Fe-poor one (grt1) (Fig. 3d). Chlorite, which replaces clinopyroxene during alteration, shows highly variable FeO contents and occurs as patchy and elongated crystals within the silicate matrix and along chromite grain boundaries (Fig. 3a-f).

4.2. Mineral chemistry

The following paragraph summarizes the main compositional features of spinels, silicates and Ti-bearing phases. Complete microprobe analyses are reported in the Supplementary Materials.

4.2.1. Cr-spinel composition

Unaltered chromite grains, selected from pristine chromitite cores, display variable compositions (SM1 Table 1). Cr_2O_3 contents range from 48.32 to 60.40 wt%, Al_2O_3 from 11.95 to 18.38 wt% and Fe_2O_3 from 0.77 to 7.70 wt%. MgO and FeO contents fall within the 6.73–15.38 wt% and 12.00–24.42 wt% ranges respectively. Mg# [=Mg/(Mg + Fe^{2+})] ranges from 0.332 to 0.691, with an average of 0.57, whereas Cr# [=Cr/(Cr + Al)] varies from 0.660 to 0.772, with an average 0.697. About trace element compositions, Ti ranges between 527 and 791 ppm, V between 1085 and 1462 ppm, Mn between 1235 and 4269 ppm, Co between 210 and 416 ppm, Ni between 318 and 1046 ppm, Zn between 420 and 2283 ppm and Ga between 21 and 32 ppm (SM2 Table 1) (Fig. 9).

Ferrian chromite displays highly variable compositions, from Fe^{2+}-enriched varieties to Fe^{2+}- Fe^{3+}-rich Cr-magnetites. Cr_2O_3 contents range between 16.19 and 65.27 wt%, Al_2O_3 between 0.30 and 17.20 wt % and Fe_2O_3 from below detection limit to 54.71 wt%. MgO and FeO contents are within the ranges of 0.8–12.00 wt% and 15.47–30.68 wt% respectively. Mg# is generally lower than that of unaltered chromite (0.044–0.590) with an average of 0.298, whereas Cr# ranges from 0.667 to 0.990, with an average of 0.854.

Chromites from the Outer, Mixed and Inner zones display a peculiar mineral chemistry, deviating from typical ferrian chromite alteration trends and with anomalous TiO_2 and V_2O_3 enrichments. A visual summary of major element variation from unaltered chromite toward the contact with rodingite is provided in Fig. 4.

Chromite of the Outer Zone is characterized by Cr_2O_3 contents ranging from 30.34 to 46.20 wt%, Al_2O_3 from 12.63 to 30.21 wt% and

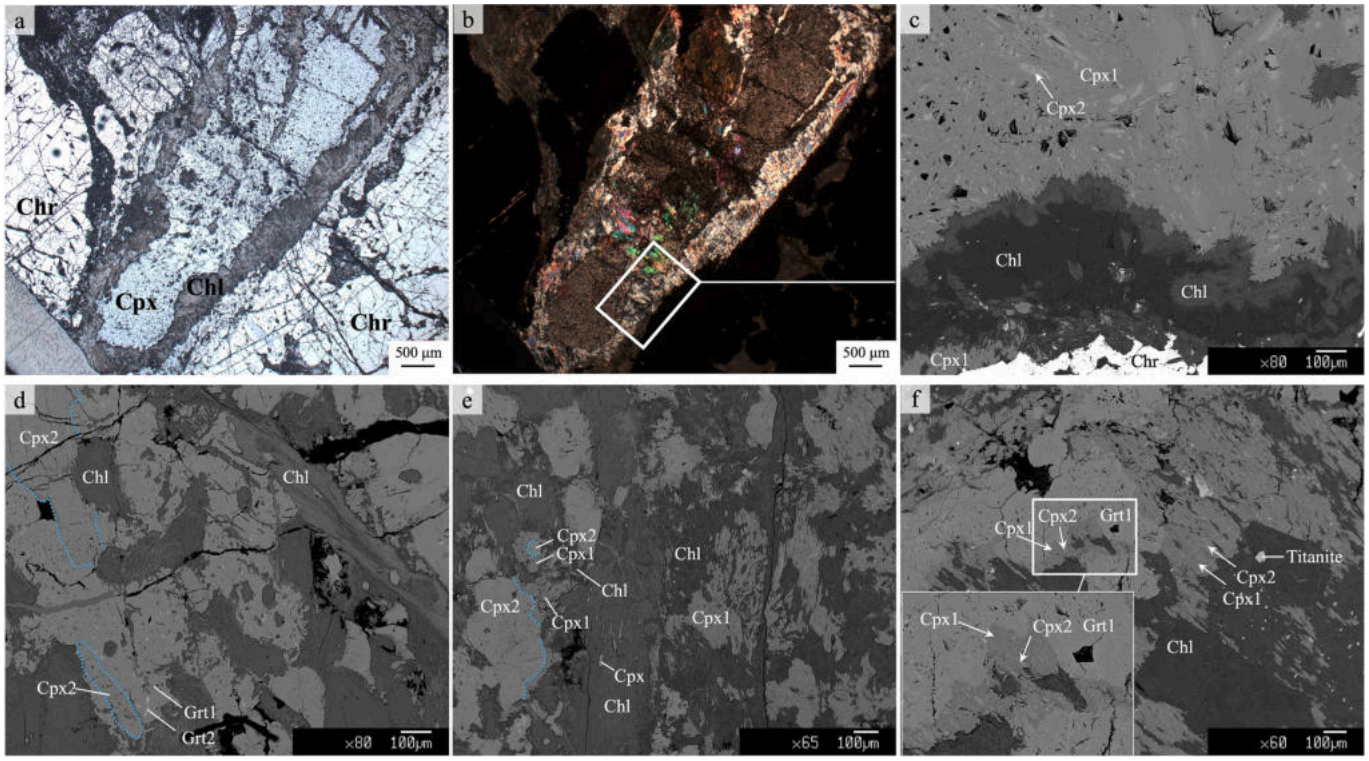

Fig. 3. Textural details of rodingite associated to Ti- V-rich chromitites; (a) reflected light and (b) crossed polarized light microphotograph of the contact between chromitite and silicate host rock; (c) BSE image showing a detail of the contact; (d), (e), (f) BSE images showing the relationship between clinopyroxene, hydrogrossular and chlorite in rodingite. Mineral abbreviations are chr: chromite, cpx: clinopyroxene, chl: chlorite, grt: hydrogrossular garnet.

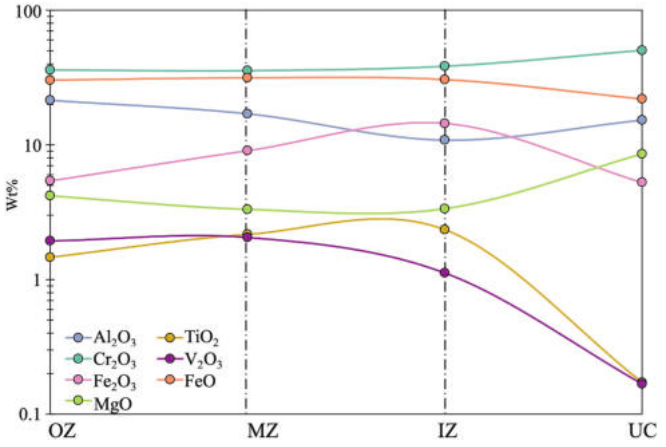

Fig. 4. Major element variation (average value) of chromite from the contact with rodingite (Outer Zone) inwards (unaltered chromite). Data are from samples D17 and D24. OZ: outer zone, MZ: mixed zone, IZ: inner zone; UC: unaltered chromite.

Fe_2O_3 from below detection limit up to 14.80 wt%. MgO and FeO contents are within the ranges of 1.75–8.13 wt% and 25.12–34.66 wt% respectively. TiO_2 content varies between 0.11 and 6.14 wt%, with an average of 1.46 wt%, whereas V_2O_3 ranges between 0.76 and 3.52 wt%, with an average of 1.93 wt%.

Chromite from the Mixed Zone is characterized by Cr_2O_3 contents ranging from 28.28 to 49.14 wt%, Al_2O_3 from 6.73 to 27.05 wt% and Fe_2O_3 contents from below detection limit up to 20.09 wt%. MgO and FeO contents are within the ranges of 0.85–6.58 wt% and 25.65–36.05 wt% respectively. TiO_2 content varies between 0.16 and 5.40 wt%, with an average of 2.16 wt%, whereas V_2O_3 ranges between 0.20 and 4.44 wt %, with an average of 2.05 wt%.

Chromite from the Inner Zone is characterized by Cr_2O_3 contents ranging from 26.95 to 49.59 wt%, Al_2O_3 from 6.78 to 17.57 wt% and Fe_2O_3 from 8.20 to 21.78 wt%. MgO and FeO contents are within the ranges of 1.01–5.80 wt% and 26.16–35.21 wt% respectively. TiO_2 content varies between 0.30 and 3.96 wt%, with an average of 2.35 wt %, whereas V_2O_3 ranges between 0.08 and 3.95 wt%, with an average of 1.12 wt%.

Trace element concentrations in spinels from the Outer, Inner and Mixed Zones are highly variable. Mn ranges between 1973 and 7940 ppm, Co between 243 and 532 ppm, Ni between 337 and 5959 ppm, Zn between 757 and 2856 ppm and Ga between 30 and 177 ppm.

4.2.2. *Silicate and Ti-oxide compositions*

The silicate matrix of massive chromitite and serpentinized dunite is predominantly composed of serpentine, olivine relicts, clinopyroxene and chlorite. One massive chromitite sample (D14) hosts abundant Cr-garnet and chlorite. The two samples showing anomalous Ti and V enrichment and their associated rodingites (D17 and D24) are enriched in clinopyroxene, hydrogrossular, chlorite and minor titanite, rutile and ilmenite.

Olivine (SM1 Table 2) is relatively common within serpentinized dunite even though it occurs exclusively as small relict grains, and it is rare within chromitite. In serpentinized dunite, MgO and FeO contents range from 50.86 to 51.57 wt% and from 7.81 to 8.22 wt% respectively. The single olivine relict detected in disseminated chromitite shows higher MgO (54.92 wt%) and lower FeO (3.32 wt%) contents.

Serpentine is the main phase replacing olivine (SM1 Table 3) and occurs in both serpentinized dunite and disseminated chromitite. In serpentinized dunite, serpentine is characterized by MgO contents ranging from 38.78 to 41.12 wt% and FeO_{tot} from 4.24 to 5.59 wt%. In disseminated chromitite, serpentine shows similar MgO contents (39.28–40.42 wt%) but lower FeO_{tot} contents (1.10–2.82 wt%).

Clinopyroxene is compositionally a diopside (Fig. 5a) (SM1 Table 4) and occurs in Ti- V- rich chromitites and associated rodingites (samples D17 and D24), as well as within serpentinized dunite (sample D23). In serpentinized dunite, clinopyroxene has MgO contents ranging from 17.66 to 18.09 wt%, FeO from 0.73 to 1.39 wt% and CaO from 24.34 to 26.25 wt%. Clinopyroxene within chromitite has lower MgO content (14.99–16.76 wt%), higher FeO (2.26–4.55 wt%) and similar CaO content (24.87–25.89 wt%). Rodingites contain two types of clinopyroxene. The first type (cpx1) has a composition comparable to that of chromitites, with MgO contents ranging between 13.54 and 16.75 wt%, FeO between 0.71 and 5.59 wt% and CaO between 20.52 and 25.88 wt %. The second type (cpx2) shows lower MgO contents (10.88–14.73 wt %), higher FeO (7.56–10.71 wt%) and CaO contents between 21.76 and 24.76 wt%.

Garnet (Fig. 5b) (SM1 Table 5) occurs in both massive chromitites and rodingites, and it is a solid solution between grossular and uvarovite end-members. In massive chromitites, garnet is associated with chromite and chlorite (Fig. 2g), and it is characterized by Al_2O_3 contents between 6.46 and 15.05 wt%, Cr_2O_3 between 9.04 and 18.76 wt%, Fe_2O_3 up to 3.91 wt% and CaO between 34.84 and 36.19 wt%. Garnet analyses from chromitites associated to rodingites and from rodingites consistently close below 100 wt% (97.29 wt% on average), indicating the presence of hydrogarnets. In chromitites associated with rodingites, garnet is characterized by Al_2O_3 contents between 17.13 and 19.84 wt %, Cr_2O_3 up to 3.23 wt%, Fe_2O_3 up to 2.28 wt% and CaO between 36.95 and 37.35 wt%. Rodingites contain two types of garnet, identified based on their Fe_2O_3 content. The first group (grt1), which is the most abundant, is characterized by Al_2O_3 between 13.75 and 23.26 wt%, Cr_2O_3 up to 4.7 wt%, Fe_2O_3 up to 1.81 wt% and CaO between 36.03 and 38.74 wt %. The second group (grt2) shows higher Fe_2O_3 contents (5.91–6.70 wt %) and slightly lower Al_2O_3 (18.5 wt% on average).

Chlorite (Fig. 5c) (SM1 Table 6) is a major phase in chromitites and rodingites, and was also detected in serpentinized dunite, where it occurs in association with accessory Fe-chromitized spinel. In serpentinized dunite, chlorites are classified as penninite and clinochlore and show Al_2O_3 contents between 7.31 and 11.41 wt%, Cr_2O_3 between 1.44 and 3.14 wt%, FeO between 2.11 and 5.04 wt%, and MgO between 35.38 and 39.92 wt%. Chlorites in chromitite are mainly of the clinochlore variety, with minor penninite. They are quite heterogeneous, with Al_2O_3 contents ranging between 11.82 and 21.25 wt%, Cr_2O_3 ranging between 0.75 and 7.31 wt%, FeO ranging from below detection limit up to 11.16 wt% and MgO between 24.09 and 33.86 wt%. Chlorites in rodingite are mainly clinochlore and pycnochlorite. They are characterized by Al_2O_3 contents between 14.14 and 21.48 wt%, Cr_2O_3 up to 4.19 wt%, FeO between 2.83 and 22.90 wt% and MgO between 17.66 and 30.37 wt%. Chlorite in rodingite also shows some minor enrichment in V_2O_3, up to 0.54 wt%.

Titanite (SM1 Table 7) occurs as an accessory phase in the rodingite-chromitite association. It is characterized by TiO_2 contents between 29.93 and 38.10 wt%, SiO_2 between 30.34 and 32.15 wt%, CaO between 28.14 and 29.55 wt%, Al_2O_3 between 1.34 and 3.21 wt% and Cr_2O_3 between 0.22 and 4.63 wt%. FeO is lower than 1 wt%.

Ilmenite and rutile (SM1 Table 7) were identified only within chromitites associated to rodingite. Ilmenite shows TiO_2 contents between 51.74 and 53.65 wt%, FeO_{tot} between 44.18 and 45.95 wt%, MnO between 1.05 and 2.98 wt% and Cr_2O_3 between 0.19 and 1.76 wt%. Rutile shows a homogeneous composition, with TiO_2 contents between 98.10 and 100.03 wt%.

4.3. *Principal component analysis*

The application of Principal Component Analysis to major, minor and trace element data was used as an exploratory tool to identify the main compositional covariations within the spinel dataset, and to evaluate whether these covariations are consistent with distinct geological processes. In particular, PCA was used to unravel the relative

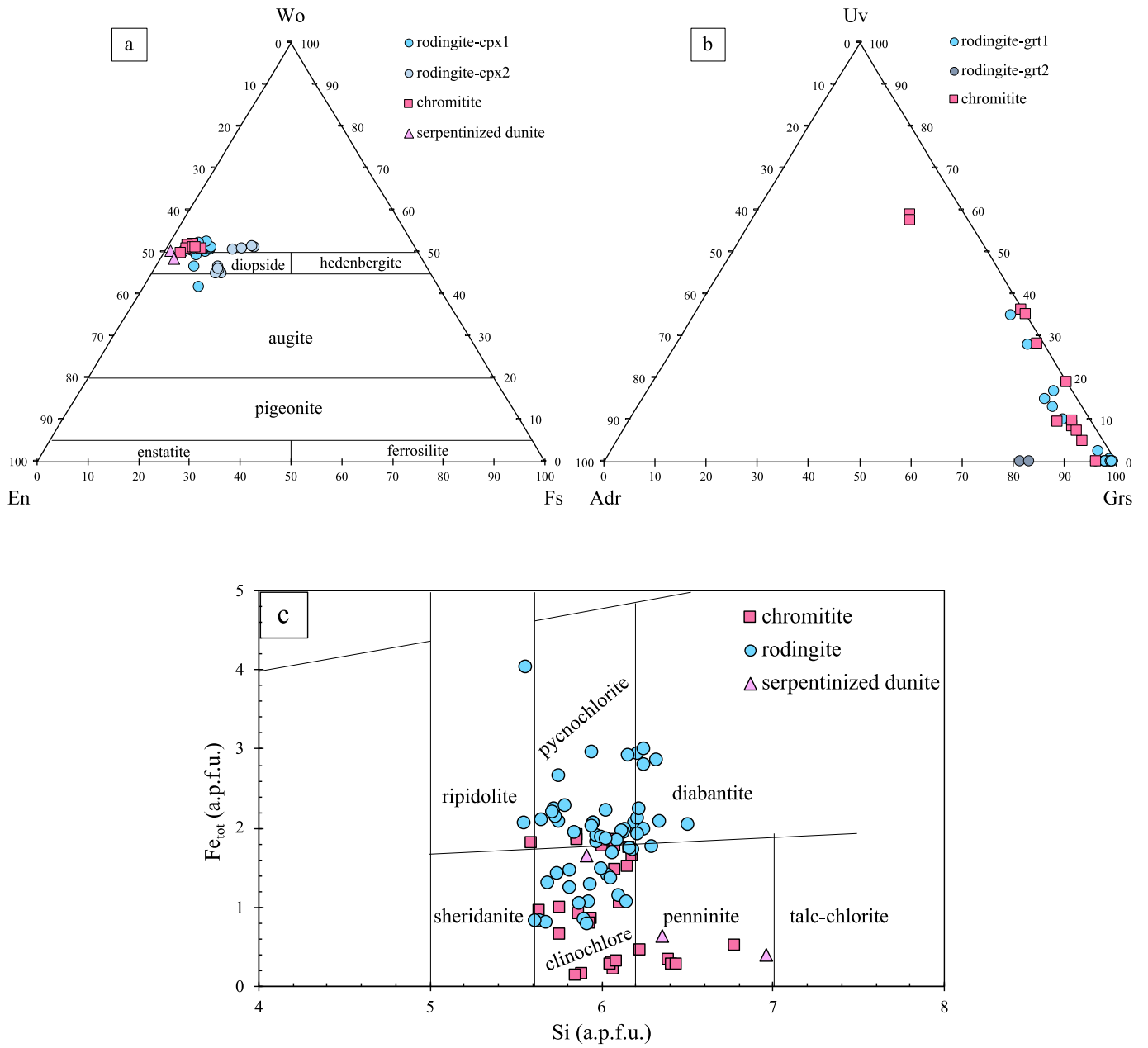

Fig. 5. Compositional diagram of (a) pyroxene, (b) garnet and (c) chlorite in chromitite, serpentinized dunite and rodingite. Chlorite compositional fields are from (Hey, 1954).

contributions of magmatic and post-magmatic processes to chromite compositional evolution. PCA does not provide genetic relationships *per se* but highlights multivariate trends that can be subsequently tested against petrographic, textural and geochemical constraints. PCA was first applied to major and minor element compositions (Fig. 6a), using Al_2O_3, Cr_2O_3, Fe_2O_3, V_2O_3, TiO_2, MgO, MnO and FeO as variables, represented as vectors in the PC biplot. The first two components, PC1 and PC2 account for approximately 71% of the total variance. PC1 captures the largest portion of the variance. Along this axis, MgO and Cr_2O_3 show a positive covariance (Fig. 6a), indicating that these elements increase together. The MgO-Cr_2O_3 group is negatively correlated with V_2O_3, TiO_2, FeO and MnO, defining an opposing trend. PC2 is mainly controlled by Al_2O_3 and Fe_2O_3, with Al_2O_3 plotting in the positive part of the PC2 axis and Fe_2O_3 plotting in the negative part. Because the covariance between two element concentrations reflects how similarly they behave in the system, variables clustered together reflect the same geochemical affinities or enriching processes. Unaltered chromites plot on the positive side of PC1, whereas chromites from Outer, Mixed and Inner Zones plot on the negative part of PC1. Outer Zone chromites also plot on the positive part of the PC2 axis, whereas Fe-chromites and magnetites plot on the negative side of the axis.

PCA was subsequently applied to trace element compositions, considering two groups: unaltered chromite and Ti- V-rich chromite. The selected variables are Zn, Co, Mn, Ga, V, Ti, Ni and Sc (Fig. 6b). Along PC1, Mn, Ga, V, Ti and Ni show a positive covariance. Along PC2, Zn and Co display a positive covariance and are negatively correlated with Sc. Ti- V-rich chromites plot on the positive side of PC1, reflecting their relative enrichment in these elements, whereas unaltered chromites, on the other hand, plot on the negative side of PC1.

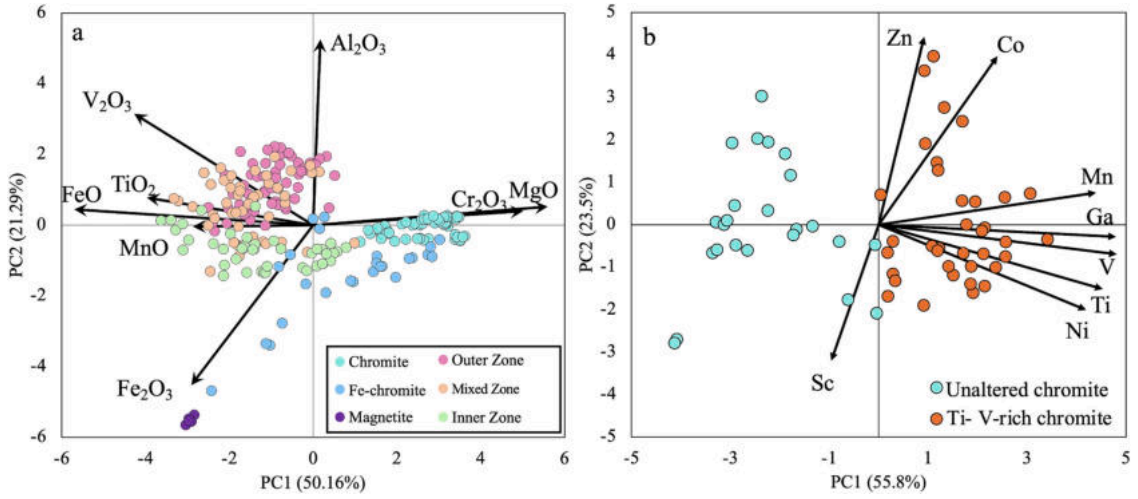

Fig. 6. PC1 *vs* PC2 biplot for (a) major and minor elements and (b) trace elements.

5. Discussion

5.1. Primary chromitite

Chromite is one of the earliest phases to crystallize during magmatic processes (Irvine, 1965; Sack and Ghiorso, 1991), making it a valuable petrogenetic indicator, especially in those lithologies where it occurs in high amounts, with large, zoned crystals that preserve information on multi-stage evolution of the system. High-Cr chromitites (chromite Cr# > 0.6) typically form from boninitic-like parent melts (Barnes and Roeder, 2001), whereas intermediate- to high-Al chromitites (chromite Cr# < 0.6) are associated with MORB-like melts (Uysal et al., 2009). The coexistence of high-Cr and high-Al chromitites is well documented in several ophiolitic massifs, including Gomati and Skyros (Greece), Bulqiza and Iballe (Albania), Mugla (Turkey), Dongbo (Tibet, China) and Sagua de Tànamo (Eastern Cuba). This association is commonly interpreted as the result of an evolving geotectonic setting, from incipient to mature subduction (Hey, 1954; Qiu et al., 2018; Saccani et al., 2017; Uysal et al., 2009; Xiong et al., 2017). Alternative interpretations include melt-rock reaction (González-Jiménez et al., 2011; Zhou and Robinson, 1994), or mechanical juxtaposition of different tectonic slices during obduction (Saccani and Tassinari, 2015).

Chromite mineral chemistry of Deva chromitites shows significant variability in terms of Cr# and Mg# (Fig. 7a), although all chromitites can be classified as high-Cr. Massive chromitites show lower Cr# (0.65–0.70) and a broader range of Mg# (0.40–0.75)compared to other podiform chromitites from the Mirdita Ophiolite (Tropoje, Kukes and Krabbi), but they partially overlap with chromitites from the Greek island of Skyros (Bussolesi et al., 2025) (Fig. 7a). Deva, Skyros and Tropoje belong to the Internal (Eastern) Ophiolites of the Vardar Domain (Saccani et al., 2011), and record boninitic, N-MORB and low-Ti tholeiitic magmatic events (Saccani and Tassinari, 2015). Chromitite

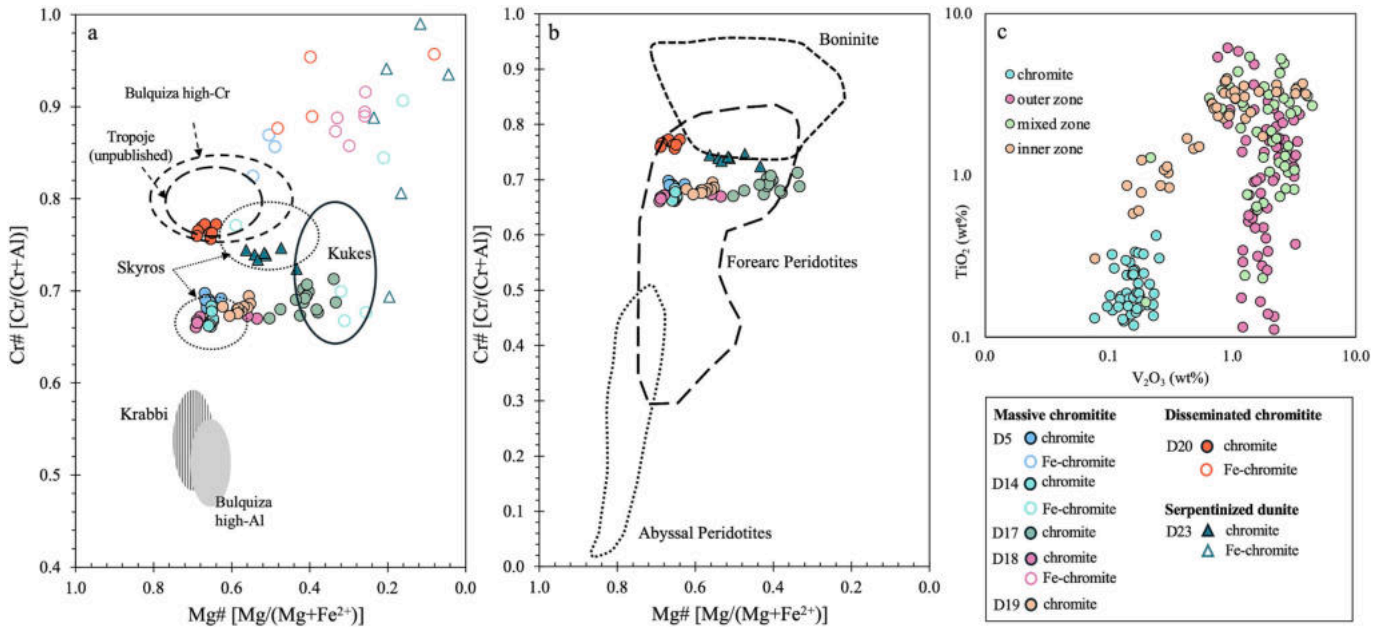

Fig. 7. (a) Chromite compositions compared with those from other Mirdita chromitites (including Bulqiza, Krabbi, Kukes and Tropoje) and Hellenic chromitites with similar characteristics (Skyros). Chromite chemistry data are sourced from Bulqiza (Beccaluva et al., 1998; Qiu et al., 2018), Krabbi (Bussolesi et al., 2022a), Kukes (Mikrut et al., 2024), Tropoje (unpublished data), Skyros (Bussolesi et al., 2025); (b) Chromite compositional diagram showing Mg# *vs* Cr#, compared to compositional fields of abyssal peridotites (Dick and Bullen, 1984), forearc peridotites (Parkinson and Pearce, 1998) and boninites (Barnes and Roeder, 2001); (c) comparison between unaltered chromite cores and Ti- V-rich chromites from samples D17 and D24.

formation in the Eastern Mirdita sector is commonly attributed to Middle Jurassic subduction-related mantle melting, broadly coeval with boninitic magmatism during subduction initiation (Beccaluva et al., 1998; Bortolotti et al., 2002; Saccani and Tassinari, 2015).

Deva chromites plot in the compositional field of forearc peridotites (Fig. 7b) and are characterized by low Ti and V contents (Fig. 7c), indicating that chromitites are related to boninitic melts generated in a forearc tectonic setting, above a subducting slab. Chromitites in supra-subduction settings typically form in the upper mantle, where fluids deriving from the subducting slab induce partial melting of the mantle, promoting the development of interconnected dunite channels. The mixing of more evolved and primary melts is the key process responsible for the precipitation of chromitite pods in the dunite channels (Arai and Yurimoto, 1994; Cocomazzi et al., 2020; Payot et al., 2014; Spiegelman and Kelemen, 2003; Wen and Zhu, 2024). Boninite-related podiform chromitites in supra-subduction settings generally form under slightly to moderately oxidized mantle conditions, typically in the range FMQ + 0.30 up to +2.4 (Caran et al., 2010; Ma et al., 2026).

MORB-normalized trace element patterns of Ti- V-rich chromites (Fig. 8a, b) and unaltered chromites (Fig. 8c) show significant variability, primarily driven by vanadium and titanium. Ti- V-rich chromites exhibit strong Ti and V positive anomalies, along with slight enrichments in Ga, Mn and Ni. Unaltered chromites from massive chromitite display trace element patterns more consistent with typical ophiolitic chromitites (Fig. 8d), characterized by slight Zn, Co and Mn enrichments and Ga, Ni and Sc depletion. Ferrian chromitization is the most common chromite alteration process within ophiolitic chromitites (Grieco et al., 2018; Grieco and Merlini, 2012). This process initially involves a loss of Al_2O_3 leading to the formation of ferrian chromite, followed, at more advanced stages, by a loss in Cr_2O_3 resulting in the development of Cr-magnetite. Metamorphic alterations of chromite generally occur through a two-step process: an initial phase of regional serpentinization, followed by the transformation of chromite into Cr-magnetite, together with chlorite formation (Mellini et al., 2005). Some Authors argue for the formation of chlorite and ferrian chromite as the result of prograde metamorphism after a first low temperature serpentinization event (Merlini et al., 2009).

Deva chromitites and their host peridotites were affected by the circulation of low-T fluids, as evidenced by the pervasive serpentinization observed in both massive chromitites and host dunites. It is possible that after an initial serpentinization stage, the massif underwent prograde metamorphism inducing the formation of chlorite from serpentine and chromite (Merlini et al., 2009), as well as of Cr-garnet in some massive chromitites (Fig. 2g) (Bussolesi et al., 2025).

5.2. Rodingite

Chromitite pods at Deva are in contact either with serpentinized dunite, which represents the replacive dunite envelope typical of many ophiolitic chromitites (Arai and Yurimoto, 1994; Zhou et al., 1996), or with rodingite. The chromitite-rodingite contact was detected in two out of eight samples collected from the mine debris, as mining tunnels are no longer accessible. This limited number of observations is not representative of the frequency and spatial distribution of chromitite-rodingite contacts in the area; therefore, the following discussion pertains the processes occurring in the area and their petrogenetic meaning, rather than the spatial extent of such processes.

Rodingites are Ca-rich metasomatic rocks, formed through the alteration of mafic dykes or gabbroic rocks by circulating fluids, typically derived from serpentinization of ultramafic rocks (Hatzipanagiotou et al., 2003). When ultramafic rocks react with water during serpentinization, the breakdown of primary minerals such as clinopyroxene and olivine releases Mg, Ca and Al into the fluids (Leach and Rodgers, 1978). These fluids can infiltrate surrounding mafic protoliths and react with them, resulting in an enrichment in Ca and Al and a depletion in Si (Hatzipanagiotou et al., 2003; Kobayashi and Kaneda, 2010; Ran et al., 2025; Rogkala et al., 2022; Tsikouras et al., 2009). As a result, primary minerals such as plagioclase and pyroxene are replaced by Ca—Al silicates. The typical assemblage encompasses hydrogarnet, clinopyroxene (diopside, augite), chlorite, with accessory phases such as vesuvianite, titanite, epidote, prehnite and zoisite (Li et al., 2004, 2017; Tang et al., 2018; Wang et al., 2019).

Deva rodingite consists of clinopyroxene, hydrogrossular and chlorite, as well as titanite as accessory phase. The protolith was likely a

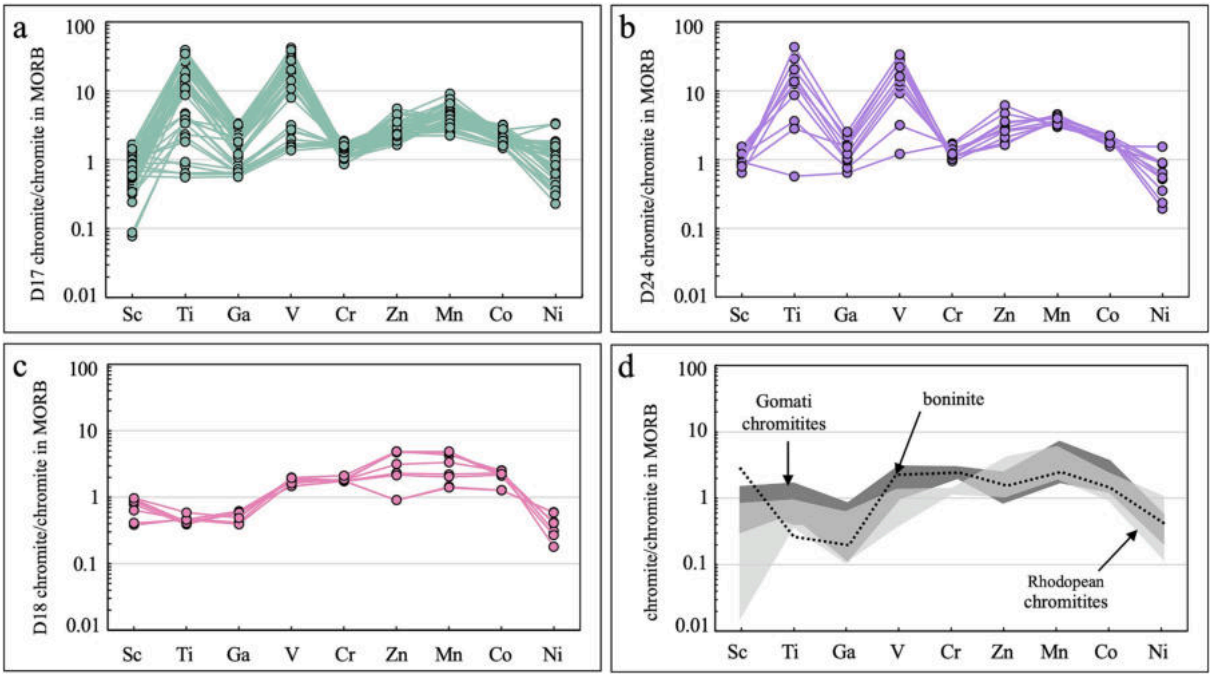

Fig. 8. Normalized spider diagrams of selected elements within Ti-V-rich chromite (a) and (b) unaltered chromite (c), compared to chromite from high-Cr chromitites from Gomati (Bussolesi et al., 2020, 2022b) and Rhodope Massif (Colás et al., 2014), and spinels in boninite (Page and Barnes, 2009); analyses are normalized to chromite in MORB.

mafic dyke, consistent with the geologic setting of the Mirdita Ophiolite, where peridotite bodies are often reported as juxtaposed or crosscut by mafic bodies, namely doleritic dykes, gabbroic intrusions and sheeted dyke complexes (Dilek et al., 2008; Saccani and Tassinari, 2015). Several types of mafic dykes and gabbroic intrusions cutting the peridotites represent later magmatic stages. Although the Eastern Mirdita ophiolite is generally associated with low-Ti magmatism (Bébien et al., 2000), there are instances of high-Ti MOR-type plutonic rocks interlayered within the SSZ intrusive sequence (Saccani and Tassinari, 2015).

Based on documented Phanerozoic rodingites, clinopyroxene with lower FeO contents may represent the original, magmatic clinopyroxene (Hatzipanagiotou et al., 2003; Karkalis et al., 2022), or an early rodingitic neoblastic phase (Frost and Beard, 2007). Based on the texture, showing coarse, anhedral crystals and the association with hydrogrossular, cpx1 was probably formed during the first stages of rodingitization. In contrast, clinopyroxene with higher FeO contents is interpreted as a later neoblastic phase, associated with more advanced stages of rodingitization (Abuamarah et al., 2025; Karkalis et al., 2022; Leach and Rodgers, 1978). Hydrogrossular is also attributed to the early stages of rodingitization, and it forms through the breakdown of plagioclase in the presence of Ca-rich Si-depleted fluids (Hatzipanagiotou et al., 2003). Chlorite is a key phase in rodingites, and its composition reflects the progressive metasomatic stages of rodingite evolution. The early stages are typically characterized by chlorite with low FeO contents (Hey, 1954), whereas more Fe-rich chlorite forms at later stages through the breakdown of grossular and diopside. These later chlorites are classified as clinochlore and penninite, which represent the majority of the chlorite crystals detected at Deva.

Initial rodingitization at Deva resulted in the breakdown of primary phases (likely plagioclase and clinopyroxene), triggered by the influx of Ca-rich, Si-poor fluids released during serpentinization of the mantle host rock. These reactions led to the formation of clinopyroxene (cpx1), hydrogrossular (grt1) and chlorite. As serpentinization progressed and the ultramafic host continued to react with water, the fluids became more Mg- and Fe-rich, leading to formation of Fe-rich neoblastic clinopyroxene (cpx2), chlorite and hydrogrossular (grt2).

Rodingitization processes occur over a range of temperature spanning from 200 to 500 °C (Li et al., 2004; Tang et al., 2018; Tsikouras et al., 2009; Wang et al., 2019), under low oxygen fugacity conditions, consistent with serpentinization, generally below the FMQ buffer (Frost and Beard, 2007). During rodingitization, element mobility is strongly controlled by fluid composition and temperature, with Ca, Mg and Si being highly mobile, whereas high-field strength elements such as Ti are generally immobile and retained in pre-existing phases or locally redistributed to form titanite (Abuamarah et al., 2025; Frost and Beard, 2007). Although vanadium may undergo limited redistribution during hydrothermal alteration, particularly under low oxygen fugacity, significant vanadium enrichments are more typically associated to hydrothermal metasomatism or melt rock reactions. Such metasomatic enrichments are documented in systems where an external vanadium source is available, such as V-bearing protoliths derived from volcanic exhalative inputs or sediments enriched in organic matter, as evidenced by the metamorphic V- Cr- spinels of the Sludyanka Complex (Reznitsky et al., 2023). In these cases, V enrichment is also coupled with Zn enrichment. In contrast, Deva Ti- V-rich chromites display a clear decoupling between V and Zn (Fig. 6b), while Ti and V systematically covary. This behavior is inconsistent with a purely fluid-driven rodingitization process, as Ti mobility in rodingitizing systems is generally very limited and Ti is commonly sequestered into stable Ti-bearing phases such as titanite or rutile (Abuamarah et al., 2025).

5.3. Chromitite – rodingite contact: evidence of melt-rock interaction

Enrichments of Ti and V within chromite have been documented in both experimental studies (Canil, 1999; Papike et al., 2004; Righter et al., 2006) and natural systems (Abzalov, 1998; Barnes and Kunilov, 2000; Goodrich et al., 2003; Reznitsky et al., 2023). In the Deva samples, the distribution of Ti- V-rich chromite in Outer, Mixed and Inner Zones (Fig. 2h, i) indicates that interaction processes, either fluid-rock or melt-rock, occurred at the contact between chromitite and rodingite and modified the composition of chromite inwards. The modified zones have variable thickness, likely reflecting differences in element diffusivity (Fig. 2i) and they exhibit high compositional variability in terms of major and minor elements involved (Mg, Fe^{2+}, Cr, Al, Fe^{3+}, Ti and V), making it difficult to capture the full range of element mobility during interaction between fluid/melt and rock. This complexity suggests that multiple processes may have contributed to the observed chemical composition of spinels, especially in light of the peculiar silicate mineral assemblage of the host rocks.

The enrichment of chromite in V_2O_3 and TiO_2 (up to 4.44 and 6.14 wt% respectively) is quite peculiar for an ophiolitic geological setting. However, comparable enrichments have been reported in other geological settings. The studies of high-Ti spinels span from experimental to natural ones. Evidence from diverse geological settings include i) high-Ti chromite (TiO_2 up to 15 wt%) from ultramafic intrusions (Noril'sk and Talnakh), formed by reaction between an existing spinel and a Ti-rich trapped interstitial liquid (Abzalov, 1998; Barnes and Kunilov, 2000); ii) spinels with anomalous TiO_2 (up to 1.23 wt%) at the Atlantis Massif, directly linked to mafic melt impregnation (Whattam et al., 2022); iii) high-Ti spinels (TiO_2 up to 1.60 wt%) in the Oman ophiolite, associated with magma circulation (Leblanc and Ceuleneer, 1991). Collectively, these observations point to melt-rock interaction, rather than fluid-driven processes, as the primary mechanism for Ti enrichement. The occurrence of ilmenite/rutile exsolutions further supports a magmatic origin. At high temperatures, chromite can incorporate excess cations (*e.g.*, Ti and Fe), forming metastable, non-stoichiometric solid solutions. Upon cooling, these structures reorder by exsolving stoichiometric ilmenite, in the form of lamellae dispersed in chromite (Ahmed et al., 2008; Khedr and Arai, 2016; Lattard, 1995; Tamura and Arai, 2005). The presence of ilmenite lamellae can also explain the inversion of enrichment trend between V and Ti (Fig. 4). In the Outer Zone, average Ti content is lower than that of V due to excess Ti having exsolved as rutile and ilmenite, whereas V was retained in the spinel structure. Experimental and natural studies indicate that ilmenite exsolution from Ti-rich spinel occurs under reducing conditions, at temperatures between 950 and 1150 °C, and at pressures compatibles with those of lithospheric mantle depths (Boe, 1978; Lattard, 1995; Legg, 1969). Rutile forms at lower temperatures from ilmenite decomposition (Lattard, 1995; Mitra and Samanta, 1996). During ilmenite/rutile exsolution, V and Ga tend to remain within the spinel lattice, whereas Mn preferentially partitions into ilmenite, a conclusion supported by mineral chemistry data.

Vanadium enrichment in chromite can occur in both magmatic and metamorphic environments. Vanadium may enter the spinel structure through metasomatic interactions (Radtke, 1962) and can be partially mobile during subsolidus re-equilibration, potentially driven by variations in fO_2 (Herd, 2006; Reznitsky et al., 2023). However, such processes generally do not produce V_2O_3 concentrations as high as those of Deva chromites. On the other hand, experimental studies indicate that vanadium-rich chromite typically crystallizes from high-temperature magmas, under reducing to near-neutral oxygen fugacity (Mallmann and O'Neill, 2009; Righter et al., 2006). Increasing fO_2 shifts vanadium to higher valence states, making it less compatible in chromite (Mallmann and O'Neill, 2009). Conversely, at lower fO_2 conditions, vanadium is more compatible in minerals, leading to higher partitioning coefficients in olivine, spinel and clinopyroxene (Mallmann and O'Neill, 2009;Righter et al., 2006; Shepherd et al., 2022). The systematic covariation of Ti and V in Deva chromites (Figs. 2i, 6a,b) suggests reaction with a late-stage Ti- V-rich MORB-like melt under redox conditions slightly below or near FMQ. V^{4+} is expected to dominate melt speciation between FMQ −2 and FMQ (Shepherd et al., 2022), yet V can still be incorporated into spinel largely as V^{3+} because trivalent V is

structurally favored in spinel/oxide lattices and valence adjustment occurs during partitioning *via* redox/charge-balance reactions (commonly involving $Fe^{2+} - Fe^{3+}$ exchange) while overall fO_2 remains buffered (Righter et al., 2006; Shepherd et al., 2022).

The Mirdita ophiolite records the co-existence, in space and time, of different magma types, including N-MORB, Medium-Ti Basalts (MTB), low-Ti IAT, and very low-Ti boninites (Saccani et al., 2011; Saccani and Tassinari, 2015). Although high-Ti magmatism predominantly characterizes the Western Mirdita Ophiolites, it has also been documented in the Eastern Mirdita Ophiolites. Regional geodynamic models suggest that subduction was established close to an active mid-ocean ridge (Hoeck et al., 2002; Saccani and Tassinari, 2015), allowing minor high-Ti MORB-type melts to be generated contemporaneously with boninitic magmatism and to be subsequently injected into the SSZ-type Eastern Mirdita Ophiolites (Saccani and Tassinari, 2015). On this basis, the injection of high-Ti MORB-type melts into the Eastern Mirdita ophiolitic mantle is most plausibly constrained to the Middle-Late Jurassic, coeval with active subduction (Dilek et al., 2008).

Principal Component Analysis applied to spinel major and minor element composition highlights multivariate trends that may be connected to the contribution of different geological processes. PC1 (Fig. 6a) represents the dominant compositional trend and separates two spinel groups. The first group, characterized by high Mg and high Cr contents, corresponds to primary magmatic chromite. The second group, comprising chromites from the Outer, Mixed and Inner Zones plots on the opposite side of the PC1 axis, and is characterized by enrichment in Ti, V, Fe, Mn and minor Ni and Ga (Fig. 6a, b). Bivariate plots further support these relationships (Fig. 9). Ti shows positive correlations with V, Mn, Ga and Ni in Ti- V-rich chromites, but no significant correlation with Zn and Co. Comparison between unaltered chromites and Ti- V-rich ones highlights enrichment in Ga and Ni only in the latter, whereasunaltered chromites exhibit low Ni content, as also shown in the MORB-normalized spider diagrams (Fig. 8). Zn and Co, as suggested by PCA, show no systematic relationship with Ti and V, and appear randomly distributed (Fig. 9e, f).

A further peculiar feature of Ti- V-rich rims is the increase in Al_2O_3 content from the Inner and Mixed Zone toward the Outer Zone. This enrichment contrasts with the decreasing trend of Al_2O_3 from unaltered spinel cores toward the Inner and Mixed zones (Figs. 2i, 4). The decrease in Al_2O_3 from chromite core to rim can hardly be explained by the high-T melt-rock interaction processes that enriched the rims in Ti and V. On the other hand, it is a common feature of Fe-chromitization processes, during which Al is partially removed from chromite and incorporated into newly formed chlorite. However, the subsequent increase in Al_2O_3 in the Outer Zone is decoupled from Fe-chromitization trends and appears to be specifically associated with the chromitite-rodingite interface. This strongly suggests that the Al_2O_3 increase in the Outer Zone is related to rodingitization, possibly to the release of Al_2O_3 in the fluid, following the breakup of plagioclase. The lack of correlation between Al_2O_3 and other variables, as well as its strong association with PC2 rather than PC1, further supports the interpretation that Al enrichment was not related either to magmatic crystallization or to melt-rock reaction processes, but instead reflects a distinct metasomatic overprint related to rodingitization.

5.4. Conclusions

Deva chromitites show peculiar features that record a complex multi-stage evolution, spanning high-T magmatic processes to lower-T fluid-rock interaction. The following stages can be reconstructed:

- The percolation of a boninitic-like parental melt under moderately oxidized conditions within mantle peridotites in a supra-subduction setting led to the formation of primary chromitite. This

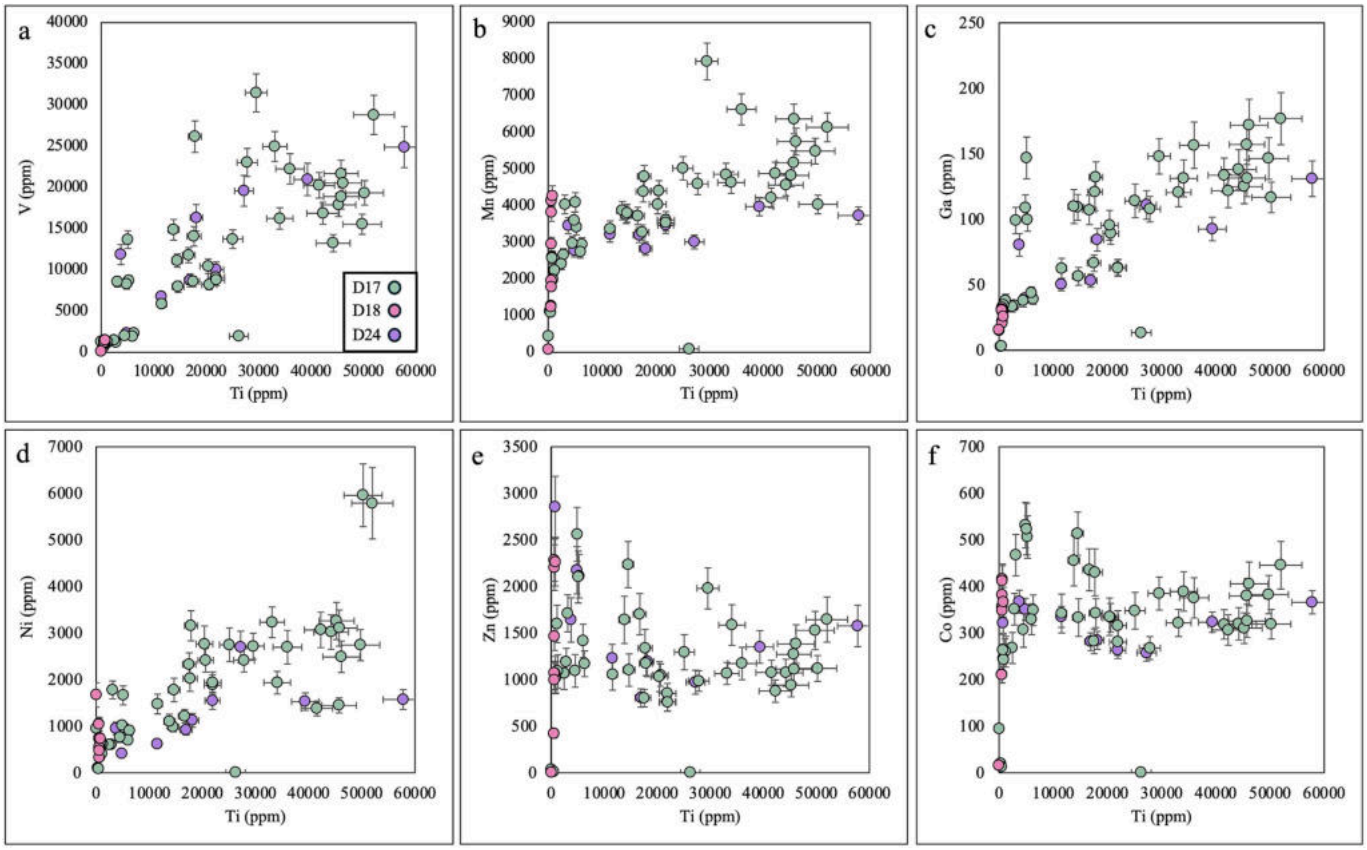

Fig. 9. Compositional variations in Deva chromites, showing Ti *vs* V, Mn, Ga, Ni, Zn and Co. Error bars indicate 2sigma uncertainties.

interpretation is consistent with the regional geodynamic setting of the Mirdita Ophiolite, where chromitite formation in the Eastern Mirdita sector is commonly attributed to Middle Jurassic subduction-related mantle melting.

- The intrusion of a Ti- V-rich mafic melt, likely of doleritic or gabbroic composition and emplaced under relatively reduced, near FMQ oxygen fugacity conditions, crosscut the chromitite bodies and affected their contact zones. Interaction between this melt and chromitite led to the formation of thick reaction zones characterized by anomalous enrichments in Ti and V along with minor enrichments in Mn, Ga and Ni. This melt was likely generated almost contemporaneously with boninitic magmatism and later injected into the SSZ-type ophiolitic mantle, during the Middle to Late Jurassic.
- During cooling, excess Ti incorporated into the chromite structure exsolved, forming rutile and ilmenite lamellae, with partial incorporation of Mn into these phases.
- The massif subsequently underwent serpentinization under redox conditions below the FMQ buffer. The fluids released during this alteration process interacted with the mafic dyke, leading to rodingitization and replacement of primary silicates by clinopyroxene, chlorite and hydrogrossular. During this stage, the release of Al from plagioclase also affected the chromitite-rodingite interface, re-enriching the spinel outer rim in Al. Fluid circulation also facilitated the mobilization of elements such as Zn and Co.

CRediT authorship contribution statement

Micol Bussolesi: Writing – review & editing, Writing – original draft, Software, Methodology, Investigation, Formal analysis, Data curation, Conceptualization. **Giovanni Grieco:** Writing – review & editing, Validation, Supervision, Resources, Project administration, Funding acquisition, Data curation, Conceptualization. **Alessandro Cavallo:** Resources, Methodology, Funding acquisition. **Qazim Hyseni:** Resources, Investigation, Formal analysis. **Federico Farina:** Methodology, Investigation, Formal analysis, Data curation.

Declaration of competing interest

The authors declare that they have no known competing financial interests or personal relationships that could have appeared to influence the work reported in this paper.

Acknowledgements

We wish to thank Dr. Sokol Mati for his precious help in finding geological information regarding the Deva area. The Authors acknowledge the support of the Italian Ministry of Education (MUR) through the project “Dipartimenti di Eccellenza 2023-2027”. We also acknowledge Andrea Risplendente for his help with EMPA analyses, and Dr. Gianluca Sessa for his help with LA-ICP-MS analyses. We thank the anonymous reviewers and the editors for their insightful comments, which helped to improve the clarity and quality of the manuscript.

Appendix A. Supplementary data

Mineral chemistry (EMPA) complete analyses, as well as Principal Component Analysis on major element, are reported in Supplementary Material 1. Complete trace element analyses and Principal Component Analysis is reported in Supplementary Materials 2. The scripts used to compute eigenvalues and eigenvectors, and to recast data onto the new PC axes are reported in Supplementary materials 3.

References

Abuamarah, B.A., Seddik, A.M.A., Azer, M.K., Chen, Y.-X., Darwish, M.H., 2025. Rodingitization of Neoproterozoic Al-Barramiya ophiolite metagabbro in the Eastern Desert of Egypt, Arabian-Nubian shield. Int. Geol. Rev. 67, 995–1013. https://doi.org/10.1080/00206814.2024.2417376.

Abzalov, M., 1998. Chrome–spinels in gabbro–wehrlite intrusions of the Pechenga area, Kola Peninsula, Russia: emphasis on alteration features. Lithos 43, 109–134. https://doi.org/10.1016/S0024-4937(98)00005-X.

Ahmed, A.H., Helmy, H.M., Arai, S., Yoshikawa, M., 2008. Magmatic unmixing in spinel from late Precambrian concentrically-zoned mafic–ultramafic intrusions, Eastern Desert, Egypt. Lithos 104, 85–98. https://doi.org/10.1016/j.lithos.2007.11.009.

Arai, S., Yurimoto, H., 1994. Podiform chromitites of the Tari-Misaka ultramafic complex, southwestern Japan, as mantle-melt interaction products. Econ. Geol. 89, 1279–1288. https://doi.org/10.2113/gsecongeo.89.6.1279.

Ballhaus, C., Berry, R.F., Green, D.H., 1991. High pressure experimental calibration of the olivine-orthopyroxene-spinel oxygen geobarometer: implications for the oxidation state of the upper mantle. Contrib. Mineral. Petrol. 107, 27–40. https://doi.org/10.1007/BF00311183.

Barnes, S.J., Kunilov, V.Y., 2000. Spinels and mg ilmenites from the Norilsk 1 and TalnakhIntrusions and other mafic rocks of the Siberian flood basalt province. Econ. Geol. 95, 1701–1717. https://doi.org/10.2113/gsecongeo.95.8.1701.

Barnes, S.J., Roeder, P.L., 2001. The range of spinel compositions in terrestrial mafic and ultramafic rocks. J. Petrol. 42, 2279–2302. https://doi.org/10.1093/petrology/42.12.2279.

Barnes, S.-J., Mansur, E.T., Maier, W.D., Prevec, S.A., 2023. A comparison of trace element concentrations in chromite from komatiites, picrites, and layered intrusions: implications for the formation of massive chromite layers. Can. J. Earth Sci. 60, 97–132. https://doi.org/10.1139/cjes-2022-0064.

Bébien, J., Dimo-Lahitte, A., Vergély, P., Insergueix-Filippi, D., Dupeyrat, L., 2000. Albanian ophiolites. I - magmatic and metamorphic processes associated with the initiation of a subduction. Ofioliti 25, 39–45.

Beccaluva, L., Coltorti, M., Ferrini, V., Saccani, E., Siena, F., Zeda, O., 1998. Petrological modelling of Albanian ophiolites with particular regard to the Bulqiza chromite ore deposits. Period. Mineral. 67, 7–23.

Boe, P., 1978. Ilmenite exsolution intergrowths in chromite from Raisduoddar–Haldi, Troms, Norway. Can. Mineral. 16, 597–600.

Bortolotti, V., Kodra, A., Marroni, M., Mustafa, F., Pandolfi, L., Principi, G., Saccani, E., 1996. Geology and petrology of the ophiolitic sequences in the Mirdita region (Northern Albania). Ofioliti 33, 135–151.

Bortolotti, V., Carras, N., Chiari, M., Fazzuoli, M., Marcucci, M., Photiades, A., Principi, G., 2002. New geological observations and biostratigraphic data on the Argolis Peninsula: paleogeographic and geodynamic implications. Ofioliti 27, 43–46.

Bussolesi, M., Grieco, G., Tzamos, E., 2019. Olivine–spinel diffusivity patterns in chromitites and dunites from the Finero Phlogopite-peridotite (Ivrea-Verbano Zone, Southern Alps): implications for the thermal history of the massif. Minerals 9, 75. https://doi.org/10.3390/min9020075.

Bussolesi, M., Zaccarini, F., Grieco, G., Tzamos, E., 2020. Rare and new compounds in the Ni-Cu-Sb-as system: first occurrence in the Gomati ophiolite, Greece. Period. Mineral. 89, 63–76. https://doi.org/10.2451/2020PM893.

Bussolesi, M., Grieco, G., Cavallo, A., Zaccarini, F., 2022a. Different tectonic evolution of fast cooling ophiolite mantles recorded by olivine-spinel geothermometry: case studies from Iballe (Albania) and Nea Roda (Greece). Minerals 12, 64. https://doi.org/10.3390/min12010064.

Bussolesi, M., Grieco, G., Zaccarini, F., Cavallo, A., Tzamos, E., Storni, N., 2022b. Chromite compositional variability and associated PGE enrichments in chromitites from the Gomati and Nea Roda ophiolite, Chalkidiki, Northern Greece. Mineral. Deposita 57, 1323–1342. https://doi.org/10.1007/s00126-022-01109-z.

Bussolesi, M., Grieco, G., Cavallo, A., 2025. The effect of multiple alteration processes on Skyros chromitites (Northern Sporades, Greece). Ofioliti 50, 1–16.

Canil, D., 1999. Vanadium partitioning between orthopyroxene, spinel and silicate melt and the redox states of mantle source regions for primary magmas. Geochim. Cosmochim. Acta 63, 557–572.

Caran, Ş., Çoban, H., Flower, M.F.J., Ottley, C.J., Yılmaz, K., 2010. Podiform chromitites and mantle peridotites of the Antalya ophiolite, Isparta angle (SW Turkey): implications for partial melting and melt–rock interaction in oceanic and subduction-related settings. Lithos 114, 307–326. https://doi.org/10.1016/j.lithos.2009.09.006.

Çina, A., 2018. Metallogenic features of chromitite mineralization related to ophiolitic assemblages, Western Balkan. In: XXI International Congress of the CBGA. Salzburg, p. 271.

Cocomazzi, G., Grieco, G., Tartarotti, P., Bussolesi, M., Zaccarini, F., Crispini, L., Science Team, O.D.P, 2020. The formation of dunite channels within harzburgite in the Wadi Tayin Massif, Oman ophiolite: insights from compositional variability of Cr-spinel and olivine in holes BA1B and BA3A, Oman drilling project. Minerals 10, 167. https://doi.org/10.3390/min10020167.

Colás, V., González-Jiménez, J.M., Griffin, W.L., Fanlo, I., Gervilla, F., O'Reilly, S.Y., Pearson, N.J., Kerestedjian, T., Proenza, J.A., 2014. Fingerprints of metamorphism in chromite: new insights from minor and trace elements. Chem. Geol. 389, 137–152. https://doi.org/10.1016/j.chemgeo.2014.10.001.

Dick, H.J.B., Bullen, T., 1984. Chromian spinel as a petrogenetic indicator in abyssal and alpine-type peridotites and spatially associated lavas. Contrib. Mineral. Petrol. 86, 54–76. https://doi.org/10.1007/BF00373711.

Dilek, Y., Shallo, M., Furnes, H., 2005. Rift-drift, seafloor spreading, and subduction tectonics of Albanian ophiolites. Int. Geol. Rev. 47, 147–176. https://doi.org/10.2747/0020-6814.47.2.147.

Dilek, Y., Furnes, H., Shallo, M., 2008. Geochemistry of the Jurassic Mirdita Ophiolite (Albania) and the MORB to SSZ evolution of a marginal basin oceanic crust. Lithos 100, 174–209. https://doi.org/10.1016/j.lithos.2007.06.026.

Fabriès, J., 1979. Spinel-olivine geothermometry in peridotites from ultramafic complexes. Contrib. Mineral. Petrol. 69, 329–336. https://doi.org/10.1007/BF00372258.
Frost, B.R., Beard, J.S., 2007. On silica activity and serpentinization. J. Petrol. 48, 1351–1368. https://doi.org/10.1093/petrology/egm021.
Ghosh, B., Morishita, T., 2011. Andradite-uvarovite solid solution from hydrothermally altered podiform chromitite, Rutland ophiolite, Andaman, India. Can. Mineral. 49, 573–580. https://doi.org/10.3749/canmin.49.2.573.
González-Jiménez, J.M., Gervilla, F., Proenza, J.A., Augé, T., Kerestedjian, T., 2009. Distribution of platinum-group minerals in ophiolitic chromitites. Trans. Inst. Min. Metall. Sect. B: Appl. Earth Sci. 118, 101–110. https://doi.org/10.1179/174327509X12550990457924.
González-Jiménez, J.M., Proenza, J.A., Gervilla, F., Melgarejo, J.C., Blanco-Moreno, J.A., Ruiz-Sánchez, R., Griffin, W.L., 2011. High-Cr and high-Al chromitites from the Sagua de Tánamo district, Mayarí-Cristal ophiolitic massif (eastern Cuba): constraints on their origin from mineralogy and geochemistry of chromian spinel and platinum-group elements. Lithos 125, 101–121. https://doi.org/10.1016/j.lithos.2011.01.016.
González-Jiménez, J.M., Griffin, W.L., Proenza, J.A., Gervilla, F., O'Reilly, S.Y., Akbulut, M., Pearson, N.J., Arai, S., 2014. Chromitites in ophiolites: how, where, when, why? Part II. The crystallization of chromitites. Lithos 189, 140–158. https://doi.org/10.1016/j.lithos.2013.09.008.
González-Jiménez, J.M., Locmelis, M., Belousova, E., Griffin, W.L., Gervilla, F., Kerestedjian, T.N., O'Reilly, S.Y., Pearson, N.J., Sergeeva, I., 2015. Genesis and tectonic implications of podiform chromitites in the metamorphosed ultramafic massif of Dobromirtsi (Bulgaria). Gondwana Res. 27, 555–574. https://doi.org/10.1016/j.gr.2013.09.020.
Goodrich, C.A., Herd, C.D.K., Taylor, L.A., 2003. Spinels and oxygen fugacity in olivine-phyric and lherzolitic shergottites. Meteorit. Planet. Sci. 38, 1773–1792. https://doi.org/10.1111/j.1945-5100.2003.tb00014.x.
Grieco, G., Merlini, A., 2012. Chromite alteration processes within Vourinos ophiolite. Int. J. Earth Sci. 101, 1523–1533. https://doi.org/10.1007/s00531-011-0693-8.
Grieco, G., Bussolesi, M., Tzamos, E., Rassios, A.E., Kapsiotis, A., 2018. Processes of primary and re-equilibration mineralization affecting chromitite ore geochemistry within the Vourinos ultramafic sequence, Vourinos ophiolite (West Macedonia, Greece). Ore Geol. Rev. 95, 537–551.
Hatzipanagiotou, K., Tsikouras, B., Migiros, G., Gartzos, E., Serelis, K., 2003. Origin of rodingites in ultramafic rocks from Lesvos island (NE Aegean, Greece). Ofioliti 28, 13–23.
Herd, C.D.K., 2006. Insights into the redox history of the NWA 1068/1110 martian basalt from mineral equilibria and vanadium oxybarometry. Am. Mineral. 91, 1616–1627. https://doi.org/10.2138/am.2006.2104.
Hey, M.H., 1954. A new review of the chlorites. Mineral. Mag. J. Mineral. Soc. 30, 277–292. https://doi.org/10.1180/minmag.1954.030.224.01.
Hoeck, V., Koller, F., Meisel, T., Onuzi, K., Kneringer, E., 2002. The Jurassic South Albanian ophiolites: MOR- vs. SSZ-type ophiolites. Lithos 65, 143–164. https://doi.org/10.1016/S0024-4937(02)00163-9.
Irvine, T.N., 1965. Chromian spinel as a petrogenetic indicator: Part 1. Theory. Can. J. Earth Sci. 2, 648–672. https://doi.org/10.1139/e65-046.
Karkalis, C., Magganas, A., Koutsovitis, P., Pomonis, P., Ntaflos, T., 2022. Multiple rodingitization stages in alkaline, tholeiitic, and calc-alkaline basaltic dikes intruding exhumed serpentinized Tethyan mantle from Evia Island, Greece. Lithosphere 2022. https://doi.org/10.2113/2022/9507697.
Khedr, M.Z., Arai, S., 2016. Chemical variations of mineral inclusions in neoproterozoic high-Cr chromitites from Egypt: evidence of fluids during chromitite genesis. Lithos 240–243, 309–326. https://doi.org/10.1016/j.lithos.2015.11.029.
Kimball, K.L., 1990. Effects of hydrothermal alteration on the compositions of chromian spinels. Contrib. Mineral. Petrol. 105, 337–346. https://doi.org/10.1007/BF00306543.
Kobayashi, S., Kaneda, H., 2010. Rodingite with Ti- and Cr-rich vesuvianite from the Sartuohai chromium deposit, Xinjiang, China. J. Mineral. Petrol. Sci. 105, 112–122. https://doi.org/10.2465/jmps.081224.
Lattard, D., 1995. Experimental evidence for the exsolution of ilmenite from titaniferous spinel. Am. Mineral. 80, 968–981.
Leach, T.M., Rodgers, K.A., 1978. Metasomatism in the Wairere serpentinite, King Country, New Zealand. Mineral. Mag. 42, 45–62.
Leblanc, M., Ceuleneer, G., 1991. Chromite crystallization in a multicellular magma flow: evidence from a chromitite dike in the Oman ophiolite. Lithos 27, 231–257. https://doi.org/10.1016/0024-4937(91)90002-3.
Legg, C.A., 1969. Some chromite-ilmenite associations in the Merensky Reef, Transvaal. Am. Mineral. 54, 1347–1354.
Li, X.-P., Rahn, M., Bucher, K., 2004. Metamorphic processes in rodingites of the Zermatt-Saas ophiolites. Int. Geol. Rev. 46, 28–51. https://doi.org/10.2747/0020-6814.46.1.28.
Li, X.-P., Duan, W.-Y., Zhao, L.-Q., Schertl, H.-P., Kong, F.-M., Shi, T.-Q., Zhang, X., 2017. Rodingites from the Xigaze ophiolite, southern Tibet – new insights into the processes of rodingitization. Eur. J. Mineral. 29, 821–837. https://doi.org/10.1127/ejm/2017/0029-2633.
Ma, H., Yang, J., Cai, P., 2026. Factors controlling the formation of high-Cr podiform chromite deposits. J. Asian Earth Sci. 299, 106958. https://doi.org/10.1016/j.jseaes.2026.106958.
Mallmann, G., O'Neill, H.St.C., 2009. The crystal/melt partitioning of v during mantle melting as a function of oxygen fugacity compared with some other elements (Al, P, Ca, Sc, Ti, Cr, Fe, Ga, Y, Zr and Nb). J. Petrol. 50, 1765–1794. https://doi.org/10.1093/petrology/egp053.
Mellini, M., Rumori, C., Viti, C., 2005. Hydrothermally reset magmatic spinels in retrograde serpentinites: Formation of "ferritchromit" rims and chlorite aureoles. Contrib. Mineral. Petrol. 149, 266–275. https://doi.org/10.1007/s00410-005-0654-y.
Merlini, A., Giovanni, G., Valeria, D., 2009. Ferritchromite and chromian-chlorite formation in mélange-hosted Kalkan chromitite (Southern Urals, Russia). Am. Mineral. 94, 1459–1467. https://doi.org/10.2138/am.2009.3082.
Mikrut, J., Matusiak-Małek, M., Ceuleneer, G., Grégoire, M., Onuzi, K., 2024. Melt-rock interaction as a factor controlling evolution of chromite and olivine in dunite - case study from the Kukes Massif (Mirdita ophiolite, Albania). J. Geosci. 49–64. https://doi.org/10.3190/jgeosci.386.
Mitra, S., Samanta, A.K., 1996. Rutile exsolution in Fe3+−chromites: a case study from layered Granulitic complex of Sittampundi, S. India. J. Geol. Soc. India 47, 75–82.
Ozawa, K., 1984. Olivine-spinel geospeedometry: analysis of diffusion-controlled Mg-Fe2 + exchange. Geochim. Cosmochim. Acta 48, 2597–2611. https://doi.org/10.1016/0016-7037(84)90308-9.
Page, P., Barnes, S.-J., 2009. Using trace elements in chromites to constrain the origin of podiform chromitites in the Thetford Mines ophiolite, Quebec, Canada. Econ. Geol. 104, 997–1018. https://doi.org/10.2113/econgeo.104.7.997.
Papike, J.J., Karner, J.M., Shearer, C.K., 2004. Comparative planetary mineralogy: V/(Cr + Al) systematics in chromite as an indicator ofrelative oxygen fugacity. Am. Mineral. 89, 1557–1560.
Parkinson, I.J., Pearce, J.A., 1998. Peridotites from the Izu-Bonin-Mariana forearc (ODP leg 125): evidence for mantle melting and melt-mantle interaction in a supra-subduction zone setting. J. Petrol. 39, 1577–1618. https://doi.org/10.1093/petroj/39.9.1577.
Payot, B.D., Arai, S., Dick, H.J.B., Abe, N., Ichiyama, Y., 2014. Podiform chromitite formation in a low-Cr/high-Al system: an example from the Southwest Indian ridge (SWIR). Mineral. Petrol. 108, 533–549. https://doi.org/10.1007/s00710-013-0317-z.
Principal Component Analysis, 2002. Springer-Verlag, New York. https://doi.org/10.1007/b98835.
Proenza, J., Sole, J., Melgarejo, J.C., 1999. Uvarovite in podiform chromitite; the Moa-Baracoa ophiolitic massif, Cuba. Can. Mineral. 37, 679–690.
Qiu, T., Yang, J., Milushi, I., Wu, W., Mekshiqi, N., Xiong, F., Zhang, C., Shen, T., 2018. Petrology and PGE abundances of high-Cr and high-Al podiform chromitites and peridotites from the Bulqiza ultramafic massif, Eastern Mirdita Ophiolite, Albania. Acta Geol. Sin. Engl. Ed. 92, 1063–1081. https://doi.org/10.1111/1755-6724.13592.
Radtke, A.S., 1962. Coulsonite, FeV2O4, a spinel-type mineral from lovelock, Nevada. Am. Mineral. 47, 1284–1291.
Ran, J., Wang, H., Yang, J., Yan, Y., Zhu, Y., Zhou, B., 2025. Petrogenesis of rodingites along the northern margin of the North China craton: constraints from zirconology and whole-rock geochemistry. Sci. China Earth Sci. 68, 750–767. https://doi.org/10.1007/s11430-024-1486-0.
Reznitsky, L.Z., Sklyarov, E.V., Barash, I.G., 2023. Metamorphic vanadian–chromian spinel (Sludyanka Complex, South Baikal Area). Ferroan spinel. Russ. Geol. Geophys. 64, 407–423. https://doi.org/10.2113/RGG20224473.
Righter, K., Sutton, S.R., Newville, M., Le, L., Schwandt, C.S., Uchida, H., Lavina, B., Downs, R.T., 2006. An experimental study of the oxidation state of vanadium in spinel and basaltic melt with implications for the origin of planetary basalt. Am. Mineral. 91, 1643–1656. https://doi.org/10.2138/am.2006.2111.
Rogkala, A., Petrounias, P., Koutsovitis, P., Giannakopoulou, P.P., Pomonis, P., Lampropoulou, P., Hatzipanagiotou, K., 2022. Rodingites from the Veria-Naousa ophiolite (Greece): mineralogical evolution, metasomatism and petrogenetic processes. Geochemistry 82, 125860. https://doi.org/10.1016/j.chemer.2021.125860.
Saccani, E., Tassinari, R., 2015. The role of MORB and SSZ magma-types in the formation of Jurassic ultramafic cumulates in the Mirdita ophiolites (Albania) as deduced from chromian spinel and olivine chemistry. Ofioliti 40, 37–56.
Saccani, E., Beccaluva, L., Photiades, A., Zeda, O., 2011. Petrogenesis and tectono-magmatic significance of basalts and mantle peridotites from the Albanian–Greek ophiolites and sub-ophiolitic mélanges. New constraints for the Triassic–Jurassic evolution of the Neo-Tethys in the Dinaride sector. Lithos 124, 227–242. https://doi.org/10.1016/j.lithos.2010.10.009.
Saccani, E., Dilek, Y., Photiades, A., 2017. Time-progressive mantle-melt evolution and magma production in a Tethyan marginal sea: a case study of the Albanide-Hellenide ophiolites. Lithosphere 10, 35–53. https://doi.org/10.1130/L602.1.
Sack, R.O., Ghiorso, M.S., 1991. Chromian spinels as petrogenetic indicators: thermodynamics and petrological applications. Am. Mineral. 76, 827–847.
Shepherd, K., Namur, O., Toplis, M.J., Devidal, J.-L., Charlier, B., 2022. Trace element partitioning between clinopyroxene, magnetite, ilmenite and ferrobasaltic to dacitic magmas: an experimental study on the role of oxygen fugacity and melt composition. Contrib. Mineral. Petrol. 177, 90. https://doi.org/10.1007/s00410-022-01957-y.
Sideridis, A., Tsikouras, B., Tsitsanis, P., Koutsovitis, P., Zaccarini, F., Hauzenberger, C., Tsikos, H., Hatzipanagiotou, K., 2022. Post-magmatic processes recorded in bimodal chromitites of the East Chalkidiki meta-ultramafic bodies, Gomati and Nea Roda, Northern Greece. Front. Earth Sci. 10. https://doi.org/10.3389/feart.2022.1031239.
Spiegelman, M., Kelemen, P.B., 2003. Extreme chemical variability as a consequence of channelized melt transport. Geochem. Geophys. Geosyst. 4. https://doi.org/10.1029/2002GC000336.
Tamura, A., Arai, S., 2005. Unmixed spinel in chromitite from the Iwanai-dake peridotite complex, Hokkaido, Japan: a reaction between peridotite and highly oxidized magma in the mantle wedge. Am. Mineral. 90, 473–480. https://doi.org/10.2138/am.2005.1570.

Tang, Y., Zhai, Q.-G., Hu, P.-Y., Wang, J., Xiao, X.-C., Wang, H.-T., Tang, S.-H., Lei, M., 2018. Rodingite from the Beila ophiolite in the Bangong–Nujiang suture zone, northern Tibet: new insights into the formation ofophiolite-related rodingite. Lithos 316–317, 33–47. https://doi.org/10.1016/j.lithos.2018.07.006.

Tsikouras, B., Karipi, S., Rigopoulos, I., Perraki, M., Pomonis, P., Hatzipanagiotou, K., 2009. Geochemical processes and petrogenetic evolution of rodingite dykes in the ophiolite complex of Othrys (Central Greece). Lithos 113, 540–554. https://doi.org/10.1016/j.lithos.2009.06.013.

Uysal, İ., Tarkian, M., Sadiklar, M.B., Zaccarini, F., Meisel, T., Garuti, G., Heidrich, S., 2009. Petrology of Al- and Cr-rich ophiolitic chromitites from the Muğla, SW Turkey: implications from composition of chromite, solid inclusions of platinum-group mineral, silicate, and base-metal mineral, and Os-isotope geochemistry. Contrib. Mineral. Petrol. 158, 659–674. https://doi.org/10.1007/s00410-009-0402-9.

Van Achterbergh, E., Ryanm, C.G., Griffin, W.L., 1999. GLITTER: on-line interactive data reduction for the laser ablation ICP-MS microprobe. In: Proceedings of the 9th V.M. Goldschmidt Conference. Cambridge, Massachusetts, p. 305.

Wang, S., Li, X.-P., Duan, W., Kong, F., Wang, Z., 2019. Record of early-stage rodingitization from the Purang ophiolite complex, Western Tibet. J. Earth Sci. 30, 1108–1124. https://doi.org/10.1007/s12583-019-1244-7.

Wang, J., Su, B., Gao, B., Li, W., Cui, M., Liu, X., Luo, Y., Pan, Q., Jia, L., Su, L., Chen, K., 2023. Four natural chromite reference materials for the determination of the first-row transition elements and gallium by LA-ICP-MS. Geostand. Geoanal. Res. 47, 683–695. https://doi.org/10.1111/ggr.12496.

Wen, X., Zhu, Y., 2024. Genesis of the sartohay podiform chromitite based on microinclusions in chromite. Minerals 14, 530. https://doi.org/10.3390/min14060530.

Whattam, S.A., De Hoog, J.C.M., Leybourne, M.I., Khedr, M.Z., 2022. Link between melt-impregnation and metamorphism of Atlantis Massif peridotite (IODP expedition 357). Contrib. Mineral. Petrol. 177, 106. https://doi.org/10.1007/s00410-022-01968-9.

Xiong, F., Yang, J., Robinson, P.T., Xu, X., Liu, Z., Zhou, W., Feng, G., Xu, J., Li, J., Niu, X., 2017. High-Al and high-Cr podiform chromitites from the western Yarlung-Zangbo suture zone, Tibet: implications from mineralogy and geochemistry of chromian spinel, and platinum-group elements. Ore Geol. Rev. 80, 1020–1041. https://doi.org/10.1016/j.oregeorev.2016.09.009.

Zhou, M.-F., Robinson, P.T., 1994. High-Cr and high-Al podiform chromitites, western China: relationship to partial melting and melt/rock reaction in the upper mantle. Int. Geol. Rev. 36, 678–686. https://doi.org/10.1080/00206819409465481.

Zhou, M.-F., Robinson, P.T., Malpas, J., Li, Z., 1996. Podiform chromitites in the Luobusa ophiolite (Southern Tibet): implications for melt-rock interaction and chromite segregation in the upper mantle. J. Petrol. 37, 3–21. https://doi.org/10.1093/petrology/37.1.3.

Zhou, M.-F., Robinson, P.T., Su, B.-X., Gao, J.-F., Li, J.-W., Yang, J.-S., Malpas, J., 2014. Compositions of chromite, associated minerals, and parental magmas of podiform chromite deposits: the role of slab contamination of asthenospheric melts in suprasubduction zone environments. Gondwana Res. 26, 262–283. https://doi.org/10.1016/j.gr.2013.12.011.